STORE&G⊃

Innovative large-scale energy storage technologies and Power-to-Gas concepts after optimisation

D6.5

Real time implementation of grid models

Due Date	31 January 2019 (M35)
Deliverable Number	6.5
WP Number	WP6
Responsible	H. Lok
Author	H. Lok (Hanze), A.Mazza (PoliTo)
Reviewer	J. Hüttenrauch (DBI)
Status	Started / Draft / Consolidated / Review / Approved / Submitted / **Accepted by the EC** / Rework

Dissemination level

✘	**PU**	Public
	PP	Restricted to other programme participants (including the Commission Services)
	RE	Restricted to a group specified by the consortium (including the Commission Services)
	CO	Confidential, only for members of the consortium (including the Commission Services)

Document history

Version	Date	Author	Description
1.0	2019-03-08	H. Lok	Titles of the sections
2.0	2019-03-19	A. Mazza	Start of report construction
3.0	2019-03-22	H.Lok, A.Mazza	First draft
4.0	2019-04-01	H.Lok, A.Mazza	Draft 2
5.0	2019-04-16	H.Lok, A.Mazza	Reviewed

Table of Contents

List of Figures

List of Tables

Acronyms

AC	Alternate Current
AVR	Automatic Voltage Regulator
CCGT	Combined-Cycle Gas Turbine
CHIL	Control Hardware-in-the-loop
CHP	Combined Heat and Power
CoE	Centre of Expertise
DC	Direct Current
DPS	Distributed Power System
DPS	Distributed Power System
DSO	Distribution System Operator
DSP	Data Signal processor
DUT	Device Under Test
ES	Electricity System
EtherCat	Power switch(es) accessible with address over Ethernet
FPGA	Field Programmable Gate Array
FTR	Financial Transmission Rights
HIL	Hardware-in-the-loop
HMI	Hardware Machine Interface
HPC	Hardware Power Control
HuT	Hardware under Test
HV	High Voltage
HW	Hardware
IEC	International Electro technical Commission
InetDistSim	Internet Distance Simulation
IP	Internet (address) Protocol
ISO	Independent System Operator
L	Coil
LC	Coil Capacitor
LCL	Coil Capacitor Coil
LV	Low Voltage
MV	Medium Voltage
OCGT	Open-Cycle Gas Turbine
OSL	Operational Security Limits
PA	Power Amplifier

P2G	Power-to-Gas
PC	Personal computer
PFD	Process Flow Diagram
PHIL	Power Hardware In the Loop
PM50F70	Power Module 50 KW
PoliTo	Power lab Torino
PtG	Power to gas
PV	Photovoltaic
PWM	Pulse Width Modulation
RES	Renewable Energy Sources
ROS	Rest of the System
RT	Real Time
RTT	Real Time Target
Sim2Sim	Simulation to Simulation
SNG	Synthetic Natural Gas
SW	Software
TCP	Transmission Control Protocol
UDP	User Diagram Protocol
VPN	Virtual Private Network

Executive Summary

The project STORE&GO aims to investigate all the aspects regarding the integration of large-scale Power-to-Gas (PtG) at European level, by exploiting it as means for long term storage. One of the aspects that should be properly addressed is the beneficial impact that the integration of PtG plants may have on the electricity system.

In the project framework, WP6 devoted its activities to investigate different aspects of the integration of PtG in the electricity grid, with the previous delivered reports.

This Deliverable is focused in particular on how to integrate the information about the facilities replicating the real world condition into a simulation environment. For doing this, the concept of Remote Hardware-in-the-loop (RHIL) has been exploited.

Remote simulation with physical hardware appears to be an effective means for investigating new technologies for the energy transition, with the purpose of solving the issues related to the introduction of new Renewable Energy Sources (RES) into the electricity system. These solutions are making the overall energy systems to be investigated much more complex than the traditional ones, introducing new challenges to the research. In fact:

- the newly integrated technologies deal with different energy vectors and sectors.

- requiring interoperability and multidisciplinary analysis.

- the systems to be implemented often are large-scale energy systems leading to enormously complicated simulation models;

- the facilities for carrying out the experiments require huge investments as well as suitable areas for proper installation.

This may lead to the fact that a single laboratory with limited expertise, hardware/software facilities and available data has not the ability to secure satisfactory outcomes. The solution is the share of existing research infrastructures, by virtually joining different distant laboratories.

This results in improvement of simulation capabilities for large-scale systems to divide into sub-systems to be run on distant targets. It will also avoid replication of already existing facilities by exploiting the remote hardware in the loop concept for testing.

Also confidential information of one lab, whose sharing may be either not allowed or require long administrative authorization procedures, can be kept confidential by simulating models locally and exchanging with the partners only proper data and simulation results through the co-simulation medium.

Up to now, the control of the electrolyser has been made by acting on the hydrogen flow through a flow controller, but the next activities will be devoted to connecting the entire local grid (electrolyser and local generation) to a power amplifier (already in the test bed) for replicating on the field the network conditions resulted from network simulation.

Thanks to the new hardware installation and the part of code developed, it was possible to send in real time measurements carried out on an 8 kW Proton Exchange Membrane (PEM) and a PV system to PoliTo, opening the possibility to properly characterize these devices. The electrolyser has been subjected to different test conditions imposed both locally and remotely.

The results reported show that the architecture developed is strong enough for being applied also in case of bigger plants. This opens the possibility to use the data for research purposed, but also to act in remote on the infrastructure in case of particular test (for example the acceptance test).

1   Introduction

New technologies or approaches are being widely developed and proposed to be deployed in real energy systems to improve desired objectives; however, supporting decision making processes to select best solutions in terms of performance and efficiently following cost-benefit analysis require some sort of scientific evidence based tools. These tools should be reliable, robust, and capable of demonstrating the behaviour and impact of newly developed devices or algorithms in different pre-defined scenarios. Therefore, new approaches and technologies need to be tested and verified using a safe laboratory test environment.

This report is about the development and realisation of some major tools and reliable methods to calculate risks and opportunities for integrating of new energy resources into the European electricity grid. Hanze University Groningen and Politecnico di Torino worked together within the STORE&GO project sharing laboratories, knowledge, hardware facilities and researchers for the realisation of the characterisation and mathematical modelling of renewable resources. Needed to realize a stable and reliable environment for remote physical hardware in the loop simulations.

For this realisation we started with the local characterisation of a PV-Field and a PEM electrolyser at Entrance Groningen by logging and measuring the electric behaviour and specific device parameters to integrate and convert these into working mathematical models of a PV-Field and electrolyser prosumer. After testing and evaluating these models by comparing the results with the real-time measurements, these test and modelling is also realised from the remote laboratory in Torino. To achieve dynamical physical hardware we also realised dynamic mathematical model(s) with real-time functionality to interact directly with the remote electrolyser. To connect both the laboratories with full duplex communication functionalities between physical hardware and models we have also realized a network which is able to share network resources on both local and remote sites.

2   Remote Hardware-in-the-loop Measurement Systems

In real-world systems, both device or approach under test and the rest of system are physical and naturally coupled. In the laboratory tests, the rest of system as the study environment is replaced with its mathematical model to simulate its behaviour. In order to couple the hardware or software under test with the virtual model of the rest of system, we need a simulation platform which guarantees the synchronization, accuracy, and stability of the overall system. To achieve this, performing real-time simulation is quite inevitable. Real-time simulation is the most reliable simulation solution mainly based on electromagnetic transient analysis which can capture dynamic behaviour of the systems in a realistic way respecting the timeline according real time occurrences.

To test and validate the performance of a device prototype or to tune or characterize a newly manufactured hardware like an electrolyser before installing in the system (e.g. connecting to power grid), a so-called hardware-in-the-loop is often carried out using digital real-time simulators. In case, the device is a controller which retrieves some measurements or alarms and produces some command signals as a feedback to the rest of system, there is no need to exchange power; hence off-the-shelf digital real-time simulator can be directly coupled with the device, performing Control Hardware-in-the-loop (CHIL). In cases, the device is a source of energy (e.g. solar panel, wind turbine connected generator, fuel cell, etc.) or sink of energy (i.e. loads), an interface is needed to enable power exchange. In such cases, a power amplifier is exploited to perform a Power Hardware-in-the-loop (PHIL).
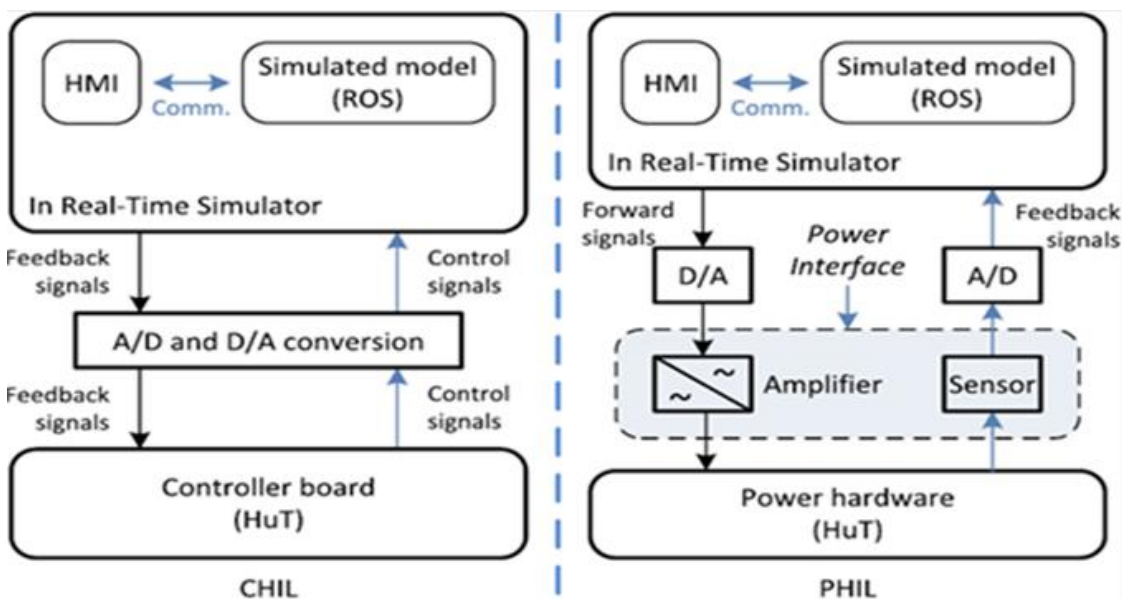
Figure 2-1: Two types of hardware in the loop

The power interface is the key element in PHIL experiments. The power interface is made of a power amplifier and a set of sensors which monitor the hardware under test (HuT). The power amplifier acts as a source or sinks in order to respectively generate or absorb power. From the simulated grid it is possible to extract the values of voltage or current to control the output of the power amplifier in order to feed the HuT. If we equip the load with current or voltage sensors, we can extract the load required current or voltage quantity and they are sent as feedback to the software grid to close the simulation loop. Moreover, a high quality of the supplied voltage to the hardware under test can be obtained if higher is the frequency bandwidth of the power interface. Wider is the output bandwidth of the Power Amplifier and better the Power Amplifier can reproduce the fast voltage oscillations (at high frequency). A narrow bandwidth means that signals at higher frequency cannot be reproduced and so they are filtered out by the power interface [1], [2].

Integrating new technologies to energy systems and interfacing different energy vectors and sectors to provide new opportunities of energy storage and management make the new systems more complex than the traditional ones. Multidisciplinary analysis is needed to ensure the right performance of a newly developed technology (e.g. prosumer, micro-grid controller, electrolyser, etc.) in the overall system. This directly introduces new challenges to the hardware-in-the-loop experiments due to the following reasons:

- New devices or technologies require interdisciplinary studies among different expertise areas;

- Interoperability analysis of newly integrated technology is crucial;

- The rest of system (i.e. simulated model of the grid) could be a large-scale energy system;

- The rest of system may be a "system of systems" with variant geographical and energy behavioural (e.g. due to social or cultural habits) characteristics;

- Interaction of OPAL[14] and Triphase[15] power amplifiers / inverters;

The remote hardware-in-the-loop system for global measurement that we established for prosumer characterization is based on the so-called "geographically distributed real-time co-simulation" [3]. This approach enables interconnecting distant laboratories to create an integrated simulation and experiment laboratory providing some benefits like virtual sharing software and hardware facilities for remote testing of devices by integrating (power) hardware in the loop and as well remote software-in-the-loop while the target model is simulated in a different lab; enhancing simulation capabilities for large-scale systems through coupling sub-systems; and Keeping susceptible data/model/algorithm confidential.

Although the vision of this approach is not limited to only remote laboratory (Hardware/Software) access, but "Internet-Distributed Hardware-in-the-loop (HIL)" has attracted many researchers since last twenty years. We intend to implement and use such an internet-distributed HIL in two steps: firstly to enable a laboratory (PoliTo's) to access Real-Time Target of the other laboratory (Hanze's), load Simulink[8] models through Internet, and run a PHIL remotely provided the hardware set-up is done (Figure 2-2 (B)); the next phase is to decouple the "rest of system" (i.e. virtual model of the grid and behavioural scenarios) to be concurrently run on simulators located in both distant laboratories (Figure 2- (C)).
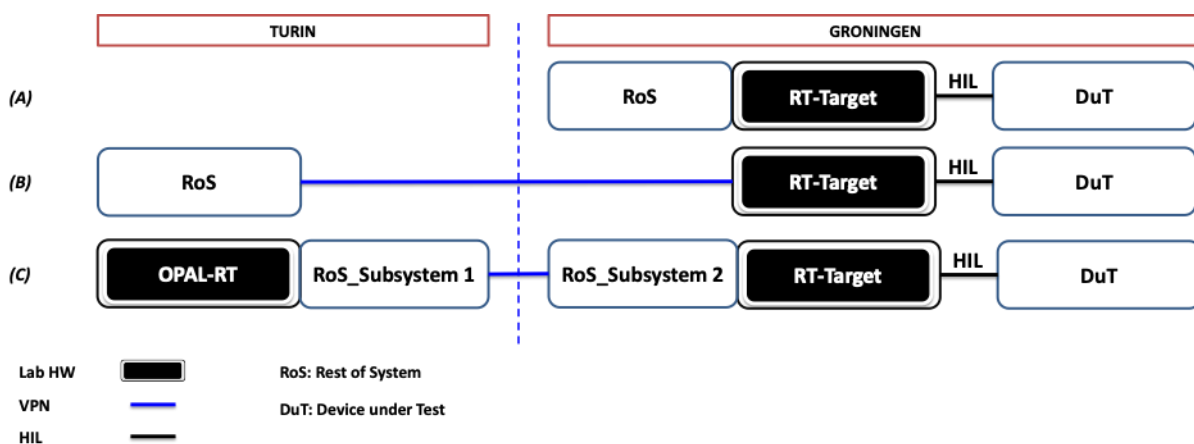
Figure 2-2 General overview of planned PHIL by PoliTo (Turin) and Hanze (Groningen) [4]

3   Hanze's Entrance facilities description and integration

3.1   Aim of the laboratory

The Real-Time Micro-Grid laboratory, situated at the Energy Transition Centre building of the Hanze University of Applied Sciences (Groningen, the Netherlands) is a test site that has been designed and built for the purpose of Energy transition- and PtG grid integration- experiments. The laboratory setup comprises new energy transition sources and all the additional components necessary to investigate the integration of hydrogen production by water electrolysis with renewable energy sources (Figure 3-1). The research method is based on the characterization of this sources, comprising electrolyser, PV panels, wind turbines, fuel cells, and others, through the acquisition of appropriate data in order to produce mathematical models based on the real-time and dynamic measurements.
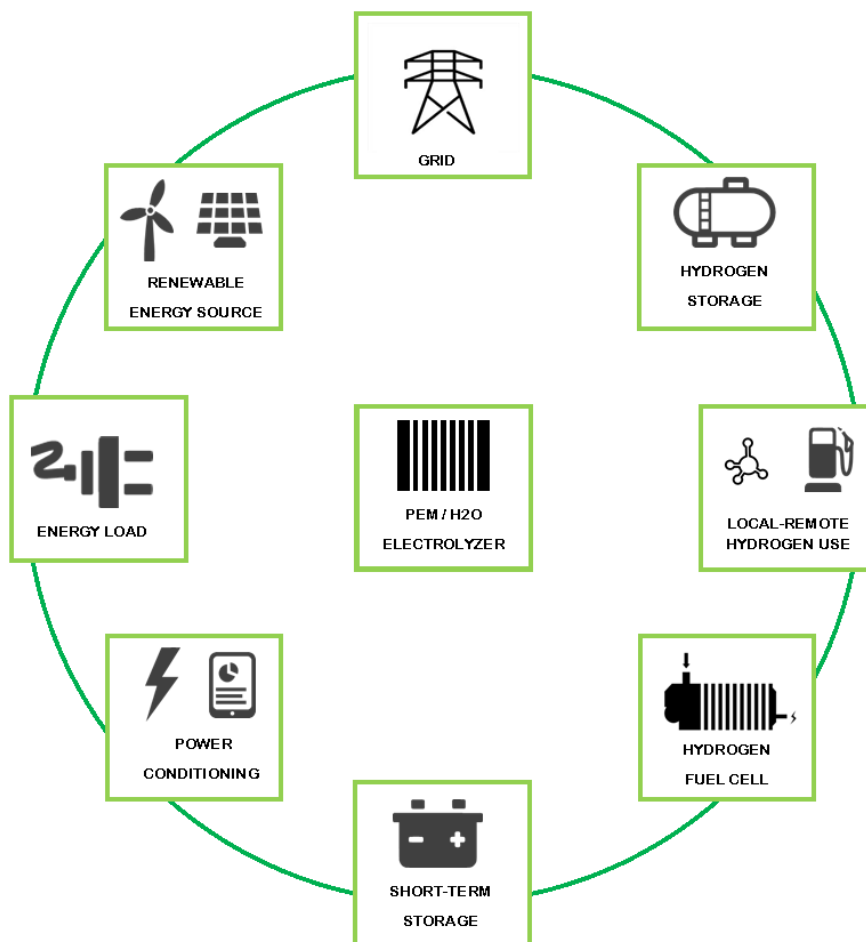
Figure 3-1: Components for the integration hydrogen production-renewable energy sources

Another important aspect is that the complete setup has now been configured to be accessible through a low latency data connection by remote use. This allows to establish a communication between the micro-grid laboratory and the Global Real-Time Simulation Lab (G-RTSLab) located at the Politecnico in Torino. In this way, the laboratory equipment in Groningen can be accessed from Turin for the purpose to remotely collect real-time data to use into large-scale grid models and with the final aim to realize a distributed real-time co-simulation. The various subsystems and both the physical and virtual connections between them are schematized in Figure 3-2.
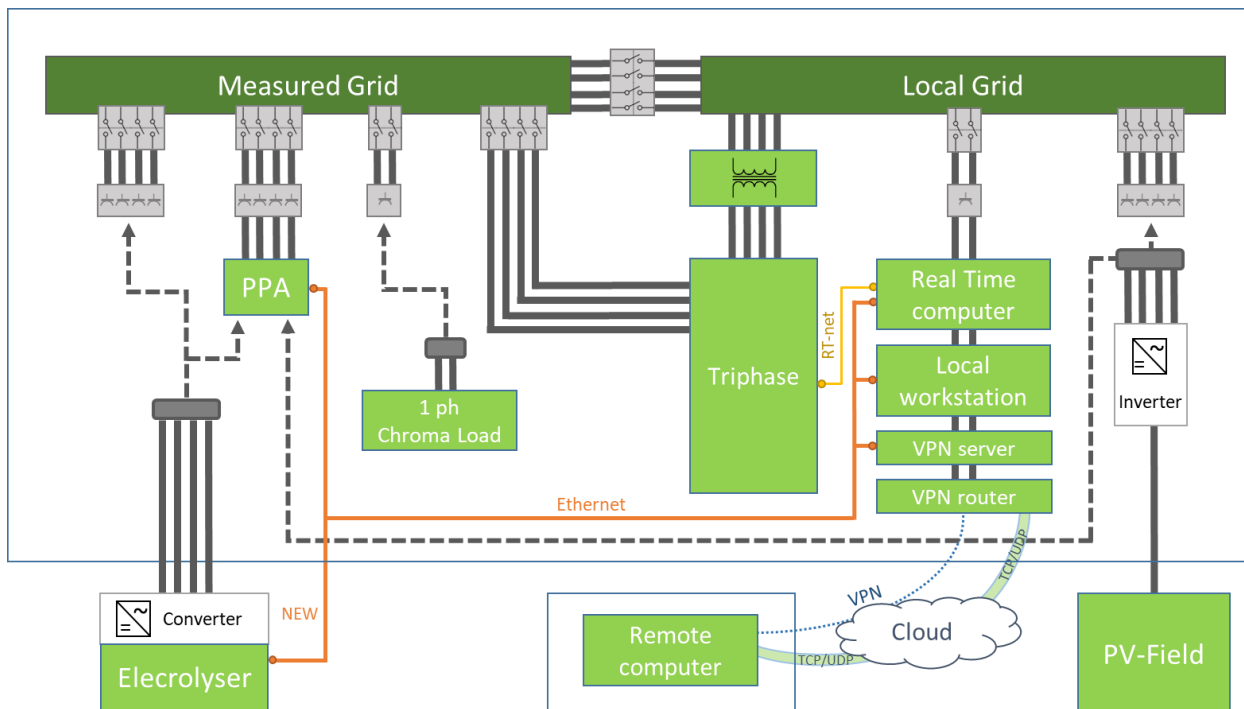
Figure 3-2: The real-time micro grid setup installed in Hanze

3.2 Grid facilities

In the lab environment, two portions of grid can be distinguished. On one side, the one called local grid is the prolongation of the main external grid and extends from the supply point of the cabin to within the laboratory room. On the other side, the one called measured grid is a main-grid independent and galvanic separated grid and occupies the main part cabin. The measured grid is configured as a three-phase with neutral conductor (3PH+N) and is functionally equivalent to the most common European three-phase AC networks. The setup is fitted with a locked switch to bypass the local grid to the micro-grid environment. After closing this switch, it is possible to connect prosumers with loads > 15 kW so that they can use and store energy from or send energy to the local grid. Connections of the single subsystems to both local and measured grid are realized and measurements are performed safely through interconnected junction box.

3.3 Power amplifier

The creation of a controllable grid (in terms of both voltage and frequency) needs a power amplifiers which is able to replicate in the grid the requested condition. In our setup, a Triphase power amplifier (PA) [9] is used. This system is able to realize a scalable, flexible and open platform for prototyping and power hardware-in-the-loop testing of power conversion and power system applications. Thus, with this system a complete controlled micro-grid is obtained.

 The PA consists of a 15 kW bidirectional isolated power module with 6-channel output, suited for bidirectional energy flow between the supply grid and single or three-phase AC or DC loads and sources. It includes power amplifiers, power converters, measurements, connection contactors, safety features, signal processing units and software libraries for high-end real-time control. For virtual operation, the PA power module is connected over a real-time communication bus, called XC real-time Network, to a powerful PC-based real-time control unit.

Figure 3-3: Interior of micro grid-lab Entrance

This PC is able to run the models for all kind of customized sources or loads in real-time. In fact, the PA can be configured as either voltage source - grid generator or current source-load, with a specific load pattern, harmonic signature, independent phase shift angel, etc. This is possible by switching over numerous internal switches with many inductive and capacitive configurable components. In particular, with a specific load model, it is possible to analyse what is needed to eliminate grid disturbances which can affect the power quality of the supply. For instance, when a certain prosumer creates a capacitive phase, the virtual model can create an inductive load which is capable to fully compensate the grid disturbance.

3.4 Electrolyser

The electrolyser connected is a fully automated Proton Exchange Membrane (PEM) based water electrolysis system of 8 kW (1 m³ hydrogen per hour at normal temperature and pressure). It is dedicated for stationary applications and can produce hydrogen continuously when supplied with power and deionized water. It is designed for indoor operation only, thus is located in a container that consists of two separated rooms. One of them contains the Power Logic Controller (PLC) and the water preparation system (where tap water is treated by reverse osmosis and ion exchange filters to create suitable water for electrolysis), whereas the other room contains the "electrolyser system", composed of:

- an electrolysis cell stack

- auxiliary equipment, necessary for regulating electrolysis operations (circulating water, drying hydrogen, pressurizing hydrogen and shutting down the system)

- sensors and control board for monitoring performance.

Furthermore, in the same room where the electrolyser is locate, a system of valves and two 5-litre tanks for storing the produced hydrogen is also installed. The tanks can be emptied afterwards by venting the contained hydrogen outside of the unit. Produced hydrogen can also be directly vented during operation, without filling the tanks.

Figure 3-4 shows the process flow diagram of the hydrogen production and the fragment inside the unit.
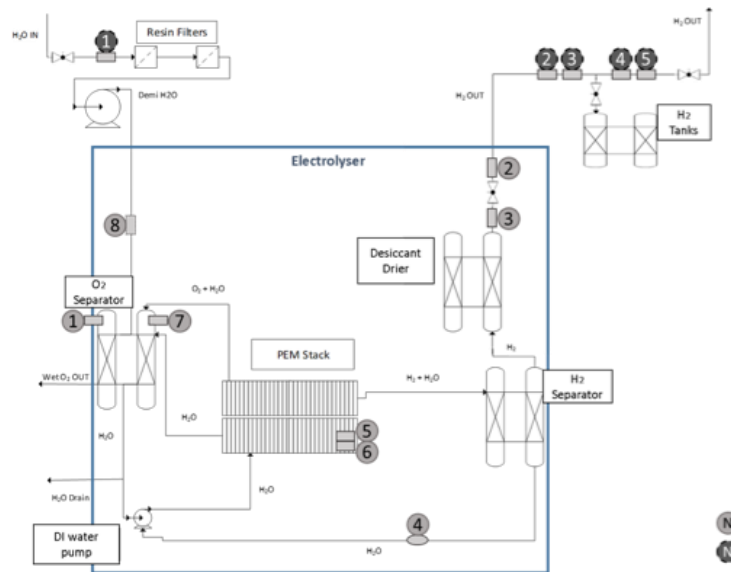
Figure 3-4: Process flow diagram of the electrolyser

The electrolyser has the following operating states:

- *Pre-Start:* The state begins when the main power switch is closed. The system flushes itself out if water quality is below the required resistivity. Water levels in the two separators (i.e., H_2/water and O_2/water) are adjusted if they are low. When Pre-Start operation is completed, it is possible to maintain this idle state or moving into the next state.

- *Generate-Vent:* In this mode, the circulation pump is started up and the system verifies the process values of water flow rate and water quality. Full current is applied to the stack after 120 seconds and hydrogen generation is started. The system checks the levels of both separator levels (i.e., H_2/water and O_2/water), voltage conditions in the stack and rectifier operation, and vents hydrogen and oxygen outside during this operation. If the process values pass all checkpoints, the electrolyser will stop venting and start to build up system pressure, leading to next state.

- *Pressurize Storage:* In this state, the hydrogen circuit in the system is pressurized up to the pressure regulator setpoint (approximately 15 bar). Once reached this pressure value, the process goes into steady-state.

- *Steady-State:* The electrolyser produces hydrogen that flows intermittently out of the system through the product hydrogen port. In fact, the hydrogen is produced and delivered only when its pressure in the tank (called product pression) is below the set point. Once the setpoint is reached, the electrolyser stops the production of hydrogen, remaining in hot stand-by. It is worth to note that if the hydrogen is not stored in the tank but only vented in the air, the electrolyser continues to produce hydrogen indefinitely.

4   Communication facilities

Realizing a remote hardware-in-the-loop needs a special infrastructure. In fact, besides the real time grid setup, it is also required a reliable low latency network: for reaching a latency lower than 50 ms it is necessary a high-speed internet connection. Furthermore, a good security for ports and connection is mandatory.
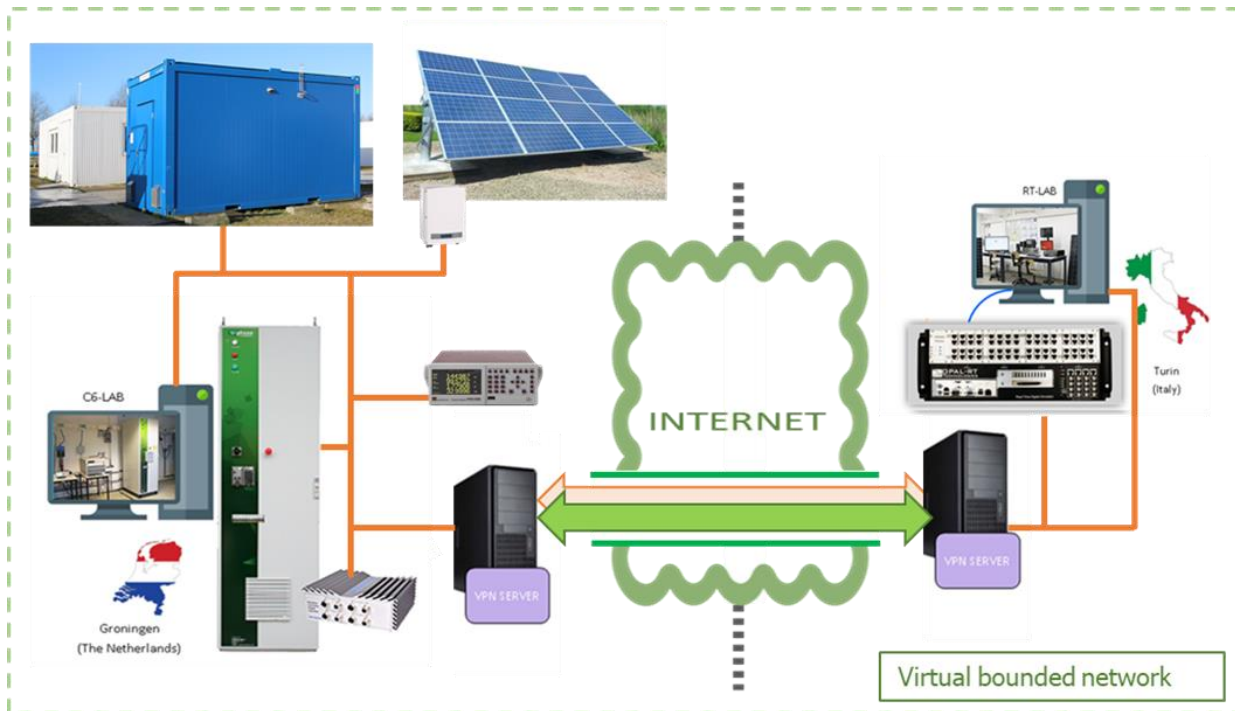
Figure 4-1: Virtual bounded network

The hardware installed at the remote site needs to be fully controllable from the co-simulation side. The use of the hardware as well as carrying out the measurements from the co-simulation requires a single Ethernet address segment: in our test bed, a virtual private network with a layer2 bridge (L2-Bridge) layer has been created to ensure a secure point to point connection in a bridged configuration.

Figure 4-1 shows the two physically separated local area networks (LAN), one placed in Groningen and the other one in Turin. They connect together different LANs, and they are merged into a single segment via a layer 2 Ethernet bridge connection [10]. In the configuration created in this test bed, Groningen is the main LAN; there is created a virtual hub on the OpenVPN server and a local bridge connection is realized to the network adapter on the specific LAN. The side of Turin represents the sub-LAN; in that side a PC connected to the Opal/RT LAN is equipped with a virtual OpenVPN server and hub which is bridged to the LAN connection. When a connection is initiated from Turin, a cascade connection is made between Turin and Groningen. At this moment, the two separated network segments are converted into a single segment, whose two sides can communicate between each other. This fact leads to have a connection between devices which seems to operate in the same network segment. So every side setup can be configured as both operate in the same LAN.
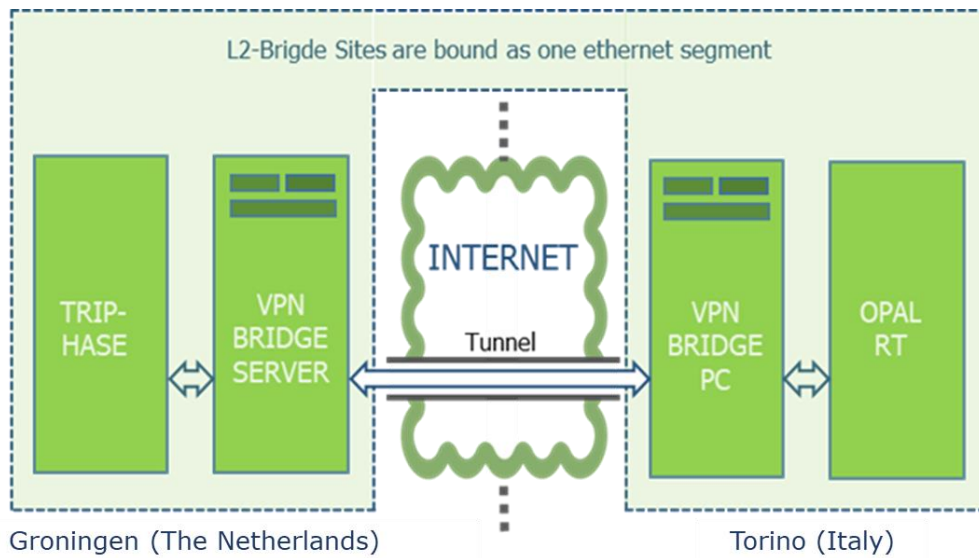
Figure 4-2: Communication structure

Software tools or math models for directly controlling real time devices (such as electrolysers, power inverters, power analyzers, and so on) use additional security protections for LAN use. These methods are usually based on the MAC-addresses or the identification number of the processor of the computer on which the tool or model is compiled or installed.

The security of the software tools mostly is related to having a valid license for the installation of the software on a specific computer. In the math models of the Triphase power system the MAC-address referring to the real-time computer is used in a combination with the identification of the workstation which uploaded the model. This security method ensures that only the user who uploaded and built the model on the real-time system can execute it. The Triphase uses a special script to realize the onetime identification of a new workstation / compiler on the realtime PC.

5 Matlab/Simulink static PV model

After the brief introduction to the technical features and functioning of electrolyser and PV panels, this chapter provides a description of the construction of the models for each element separately. These models will be added to the large-scale power grid model, scaled up and merged to create the desired global prosumer. It is important to mention that both the electrolyser and PV panels are intended to be represented into the complete Simulink model of the grid by means 'Three-Phase Dynamic Load'. It will be fully characterized the following section dedicated to the description of the main used Simulink blocks. The models implements a three-phase load with active and reactive power controlled as external input. In this way, the electrolyser is modelled as a common positive load (power drawn from the grid) while the PV panels are modelled as negative loads (power injected into the grid). It follows that the laboratory measurements performed on electrolyser and PV panels should be aimed at collecting the active and reactive power consumed by the former and produced by the latter given as input values to the mentioned block.

5.1 PV panels modelling

In this chapter(s) the construction of the mathematical models is explained. Also the use method(s) and selection of methods and algorithms to construct a most reliable model.

After the construction off the first model we concluded that the model is acceptably precise and the approach for creating it can be considered as an adequate model. However, it is not in line with some models already existing in the scientific field. Since temperature sensors were unavailable for the PV installation under study, the model does not take the temperature into account. It follows that this first model is not general but, given a generic irradiance vector as input, the outputs would reflect the real electrical PV panels behavior only throughout a limited time of the year in which the air temperature remains roughly the same. Furthermore, the model presents also a basic systemic error: since the values handled (both powers and irradiance) are energy quantities, the meaning of the energy has to be maintained in the analysis. This condition is met if the energies, obtained by integrating each variable over the measured time frame, are equal before and after the linear interpolation. So also a second method is used (section 5.4) to make the model completely optimized with also integrated temperature measurements.

5.2 Collecting real time data.

In order to build the PV panels model, the first step was to get information about the real time process data. For the PV prosumer have measured:

- PV panels produced electrical AC power is measured and logged by PPA power analyzer [11]. Measurements are logged with an interval of 5 s.
- Solar irradiance is measured by the onsite pyranometer. The pyranometer is continuously logged to a multi accessible database with an interval of 1 min.
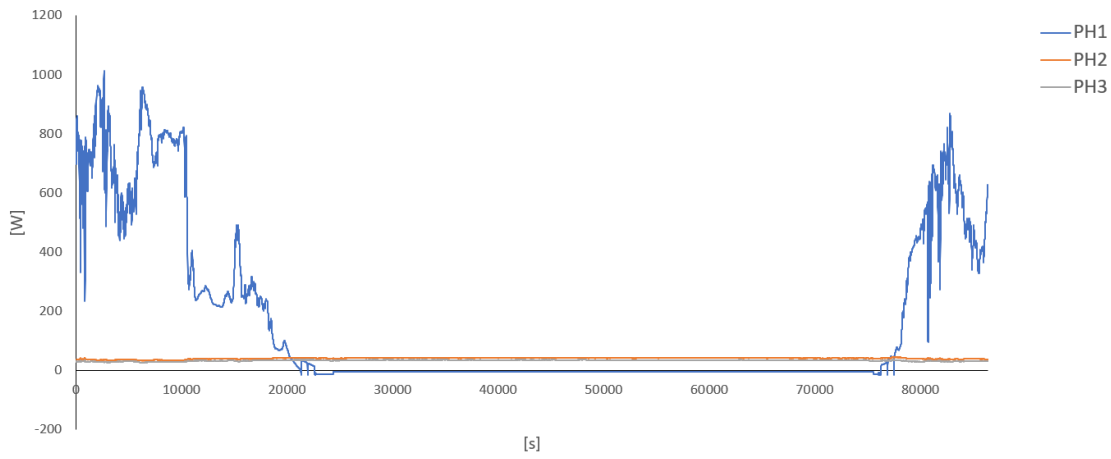
Figure 5-1: PV panels - PPA measurements: active power
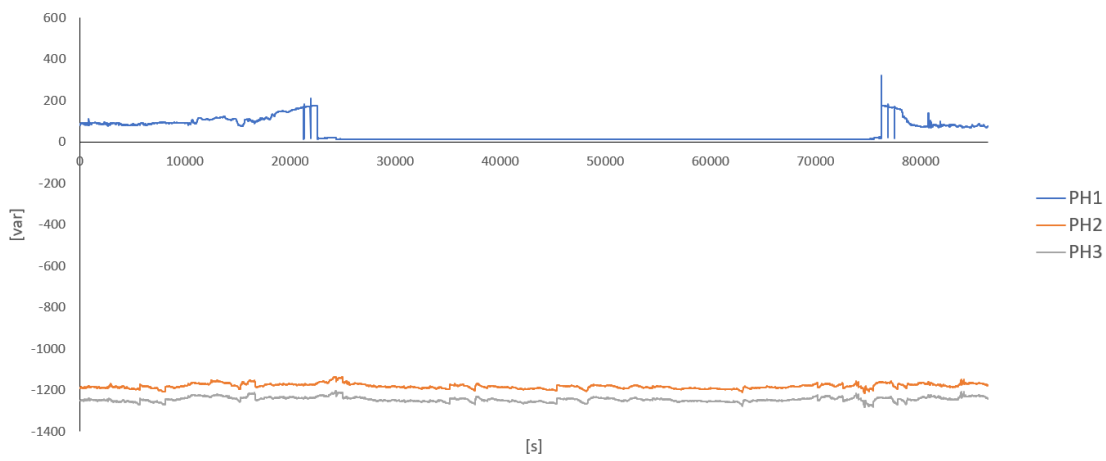
Figure 5-2: PPA measurements: reactive power
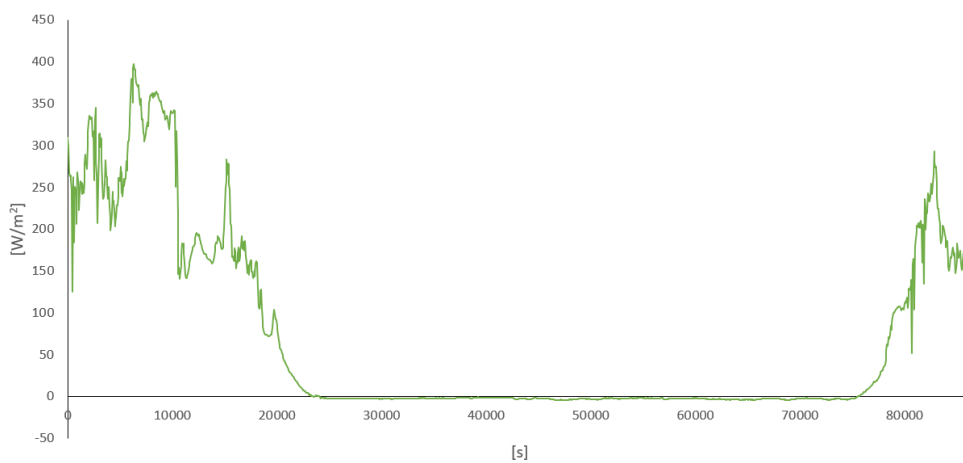
Figure 5-3: Pyranometer measurements: solar irradiance

5.3 Data analysis real time data

The measured data of active and reactive power as well as solar irradiance were transferred to Matlab for data processing operations and stored into two matrixes (named PPA_PV – for electrical data and Pyranom – for irradiance data). In particular, the matrix columns are organized as follows.

Table 5-1: PPA_PV [17279x7] (intervals of roughly 5s within 24h)

	Column 1	Column 2	Column 3	Column 4	Column 5	Column 6	Column 7
	Seconds from 0	P PH1 [W]	P PH2 [W]	P PH3 [W]	Q PH1 [var]	Q PH2 [var]	Q PH3 [var]
1.	Second 0						
2.	Second 4.931		(convention: produced power marked as negative)				
…	…						
17279.	Second 86401						

Table 5-2: Pyranom [1441x2] (intervals of roughly 1min within 24h)

	Column 1	Column 2
	Seconds from 0	Irradiance [W/m^2]
1.	Second 0	
…	…	
404.	Second 24199	
405.	Second 24260	
…	…	
1441.	Second 86400	

Since the pyranometer sampling time could not be set equal to the PPA one, it's necessary to draw new estimated data from the real measured data. Because of the non-regularity of the time steps, this was done by a combination of linear interpolation and extrapolation. First, for each set of two known data points – represented by the coordinates (x_k, y_k) and (x_{k+1}, y_{k+1}), the straight line between them (so-called linear interpolant) is constructed through the following formula:

$$\frac{(y - y_k)}{(x - x_k)} = \frac{(y_{k+1} - y_k)}{(x_{k+1} - x_k)}$$

In this way, a piecewise linear function is obtained. Then, the needed new data points – represented by the coordinates (x_n, y_n), are extrapolated from the straight line between the two known points – again given by the coordinates (x_k, y_k) and (x_{k+1}, y_{k+1}), through the following formula:

$$y_n = y_k + (x_n - x_k) \cdot \frac{(y_{k+1} - y_k)}{(x_{k+1} - x_k)}$$

In this case, x is the time variable t (along the x-axis) whereas y represents any variables among active power, reactive power and irradiance (along the y-axis).

Matlab matrix dimensions are modified as reported below.

Table 5-3: PPA_PV_lin [17281x7] (intervals of 5s within 24h, including data at time 0)

	Column 1	Column 2	Column 3	Column 4	Column 5	Column 6	Column 7
1. 2. ... 17281.	Second 0 Second 5 … Second 86400	P PH1 [W]	P PH2 [W]	P PH3 [W]	Q PH1 [var]	Q PH2 [var]	Q PH3 [var]

Table 5-4: Pyranom_lin [17281x2] (intervals of 5s within 24h, including data at time 0)

	Column 1	Column 2
1. 2. ... 17281.	Second 0 Second 5 … Second 86400	Irradiance [W/m^2]

5.4 Creation of lookup table.

As a first approach, the idea for the PV panels model was that it encompassed two look-up tables which take the irradiance values as input and provide the produced electrical power, both active and reactive, as outputs (to control the dynamic load block).

For this purpose, the needed functions are *P(irr)* and *Q(irr)*, and their independent variable – solar irradiance – must be monolithically increasing. This means that some data processing is required to get the final result. First of all, this process started by sorting the elements of the irradiance array in ascending order. In second instance, all the other measured data were rearranged in such a way to make one row of the electrical variables matrix refer to the same row of the irradiance array. The resulting matrixes can be schematized in the following way.

Table 5-5: Pyranom_lin_sort [17281x2]

	Column 1	Column 2
1. **2.** **...** **11710.** **11711.** **...** **17281.**	Second 47415 Second 47410 ... Second 19170 Second 19230 ... Second 6300	-4.2984 W/m^2 -4.2934 W/m^2 ... 72.200 W/m^2 72.200 W/m^2 ... 397.10 W/m^2

Table 5-6: PPA_PV_lin_sort [17281x7]

	Column 1	Column 2	Column 3	Column 4	Column 5	Column 6	Column 7
1. **2.** **...** **11710.** **11711.** **...** **17281.**	Second 47415 Second 47410 ... Second 19170 Second 19230 ... Second 6300	4.5231 W 4.5237 W ... -68.825 W -68.548 W ... -954.96 W	-42.0322 W -42.0055 W ... -42.440 W -42.070 W ... -33.564 W	-35.873 W -35.869 W ... -35.302 W -35.750 W ... -27.102 W	12.253 var 12.249 var ... 148.033 var 149.227 var ... 81.647 var	-1183.5 var -1183.7 var ... -1171.8 var -1172.8 var ... -1183.5 var	-1247.2 var -1247.5 var ... -1232.8 var -1235.8 var ... -1249.4 var

At the end of this process the obtained irradiance array contains increasing data values, but yet not monolithically. In fact, some subsequent cells store exactly the same value (for instance the cells within rows number 11710 and 11711, as shown in the table above representing a simplified version of the pyranometer matrix). Therefore, next step of this data processing operation consisted in deleting the irradiance matrix rows containing repetitive irradiance values, and consequently, deleting the corresponding rows of the electrical variables matrix.

At the end of this operation the resulting irradiance array contains monolithically increasing data values and can be used for building the desired look-up tables. The applied criterion can be depicted

as follows, taking the lastly obtained matrixes as reference (the row indexes are lower because some rows in-between have been deleted during the process).

Table 5-7: Pyranom_lin_sort_del [10091x2]

	Column 1	Column 2
1.	Second 47415	-4.2984 W/m^2
2.	Second 47410	-4.2934 W/m^2
…	…	…
5084.	Second 19170	72.200 W/m^2
~~**5085.**~~	~~Second 19230~~	~~72.200 W/m^2~~
…	…	…
10091.	Second 6300	397.10 W/m^2

Table 5-8: PPA_PV_lin_sort_del [10091x7]

	Column 1	Column 2	Column 3	Column 4	Column 5	Column 6	Column 7
1.	Second 47415	4.5231 W	-42.032 W	-35.873 W	12.253 var	-1183.5 var	-1247.2 var
2.	Second 47410	4.5237 W	-42.006 W	-35.869 W	12.249 var	-1183.7 var	-1247.5 var
…	Second 19170	…	…	…	…	…	…
5084.		-68.825 W	-42.440 W	-35.302 W	148.033 var	-1171.8 var	-1232.8 var
~~**5085.**~~	~~Second 19230~~	~~-68.548 W~~	~~-42.070 W~~	~~-35.750 W~~	~~149.227 var~~	~~-1172.8 var~~	~~-1235.8 var~~
…	…	…	…	…	…	…	…
10091.	Second 6300	-954.96 W	-33.564 W	-27.102 W	81.647 var	-1183.5 var	-1249.4 var

At this point, look-up tables can be constructed by placing the irradiance array along the horizontal axis and the array of the desired electrical variable along the vertical axis. This is what has been done in the model in figure 5-4 for both active and reactive power of all three phases. In order to prove the correctness of this model, the initial irradiance vector has been given unchanged as input to the whole group of look-up tables. This check could have been considered successful if the output graphs had been roughly comparable to the plots of the initial unvaried electrical variables. The comparison is made easier by making the model plot these initial variables as well.

Figure 5-4: PV panels model: method 1
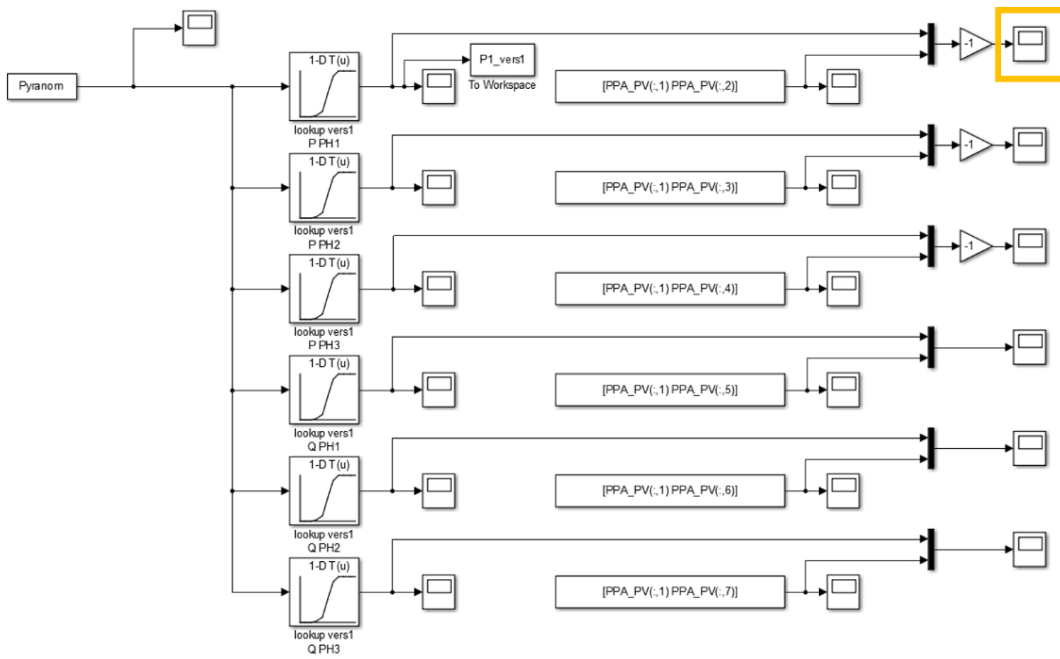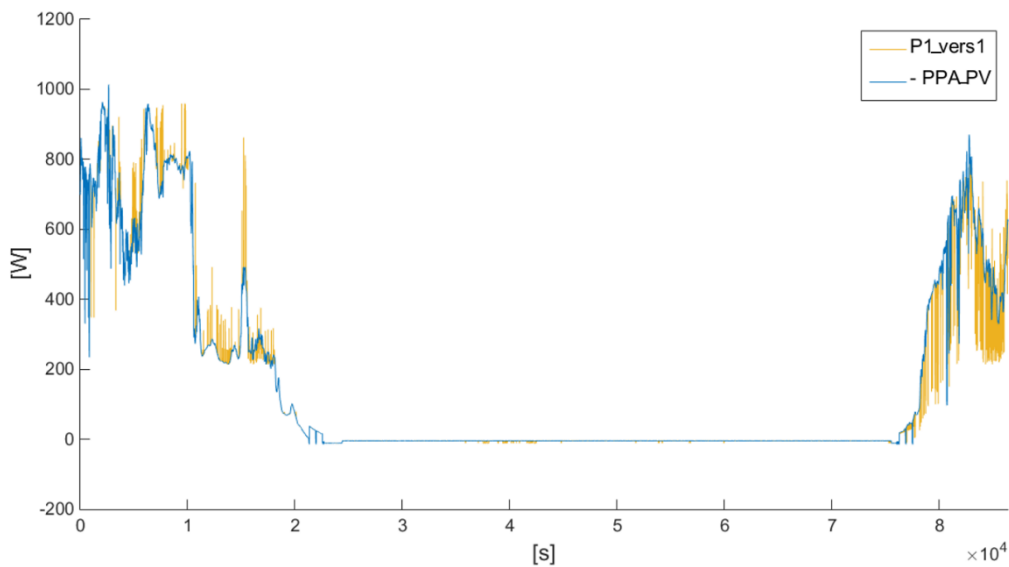

Figure 5-5: Comparison estimated and measured active power (plot method 1)

By comparing both sets of graphs as reported in figure 5-5, it is clear that the model outputs variate within a higher range and with a higher frequency than the initial data, thus it is possible to draw the conclusion that the model itself is slightly different then the data it is representing.

5.5 PV panels model (method 2)

In order to improve the model, a second calculation method in the application of the following criterion: during the iterative process of skimming through the irradiance column, every time two or more subsequent cells were found to store the same value, the mean value of the cells corresponding to the detected rows was calculated for each of the other columns/variables. This mean value was stored in the cell corresponding to the first row of the set, while the other rows were deleted. The applied criterion can be depicted once again as follows, referring to the same example for the sake of clarity.

Table 5-9: Pyranom_lin_sort_del [10091x2] (same of first method)

	Column 1	Column 2
1. **2.** … **5084.** ~~**5085.**~~ … **10091.**	Second 47415 Second 47410 … Second 19170 ~~Second~~ ~~19230~~ … Second 6300	-4.2984 W/m^2 -4.2934 W/m^2 … 72.200 W/m^2 ~~72.200 W/m^2~~ … 397.10 W/m^2

Table 5-10: PPA_PV_lin_sort_del_mean [10091x7]

	Column 1	Column 2	Column 3	Column 4	Column 5	Column 6	Column 7
1. **2.** … **5084.** ~~**5085.**~~ … **10091.**	Second 47415 Second 47410 … Second 19170 ~~Second~~ ~~19230~~ … Second 6300	4.5231 W 4.5237 W … -68.686 W ~~-68.825 W~~ ~~-68.548 W~~ … -954.96 W	-42.032 W -42.006 W … -42.255 W ~~-42.440 W~~ ~~-42.070 W~~ … -33.564 W	-35.873 W -35.869 W … -35.526 W ~~-35.302 W~~ ~~-35.750 W~~ … -27.102 W	12.253 var 12.249 var … 148.630 var ~~148.033 var~~ ~~149.227 var~~ … 81. 647 var	-1183.5 var -1183.7 var … -1172.3 var ~~-1171.8 var~~ ~~-1172.8 var~~ … -1183.5 var	-1247.2 var -1247.5 var … -1234.3 var ~~-1232.8 var~~ ~~-1235.8 var~~ … -1249.4 var

Lastly, new look-up tables can be built by taking the ones previously used and substituting the vertical axis arrays with the columns of the newly obtained electrical variables matrix. This leads to the new model in figure 5-6, where, as in the previous version of the model, the look-up tables for both active and reactive power of all three phases are present. As before, they take the unchanged initial irradiance vector as input and provide the related electrical variables as output. In order to check the precision of the model, once again each output has been compared with the corresponding initial electrical variable vector. This time, as reported in figure 5-7, it can be observed that the two groups of plots are roughly similar, surely more than in the previous case at least.
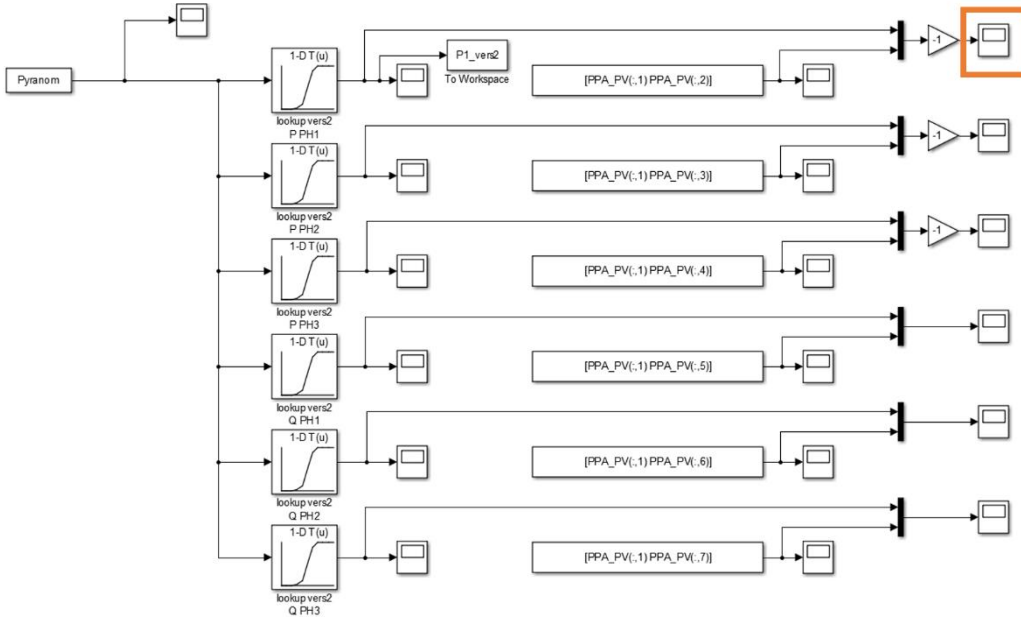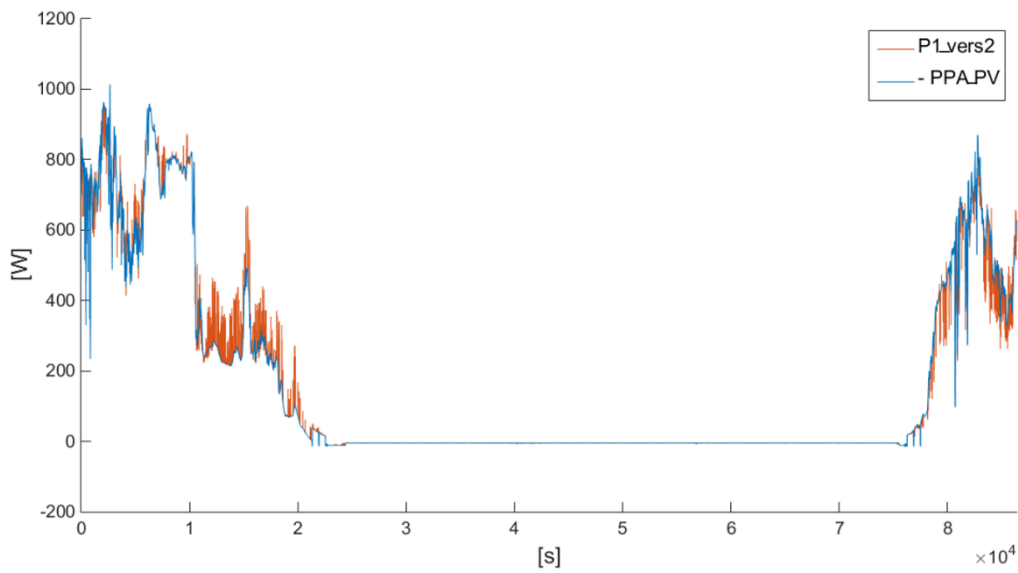
Figure 5-6: PV panels model (method 2)

Figure 5-7: Comparison estimated and measured active power (plot method 2)

5.5.1 Collecting real time data.

In order to make up for these imprecisions, the previous PV panels model has been improved by keeping the previously measured data: electrical variables obtained by means of the PPA power analyzer and solar irradiance obtained by means of the pyranometer. In addition to these data, in this case, also the temperature variable has been taken into account. In particular, since no temperature measurements are available for the PV field under study, it has been considered:

- The air temperature obtained by means of temperature sensors located on a neighbor PV installation.
- In the same way as the solar irradiance, the air temperature is measured by the associated sensors and automatically uploaded every day on the Hanze's online database. The temperature data can then be accessed and downloaded through a private Hanze's account.

The temperature measurements have been retrieved within the interval in which all the other variables have already been measured (equal to 24h, starting on last 31st October at 10:32 am and ending on 1st November at 10:32 am). Since the temperature sensors have been preprogrammed to collect everyday measurements from 5:00 am to 10:00 pm, within the desired interval the temperature data from 10:00 pm of 31st October to 5:00 am of the day after are unavailable. The temperature sensors sampling time is 5 min.

The already existing Excel files containing electrical variables and irradiance data were kept unchanged, thus also in this case the results of these measurements look the same as shown in the previous figure 5-7.

The new temperature data were imported in new Excel files, one file for each day from 5:00 am to 10:00 pm. The associated graphs are plotted in figure 5-8.
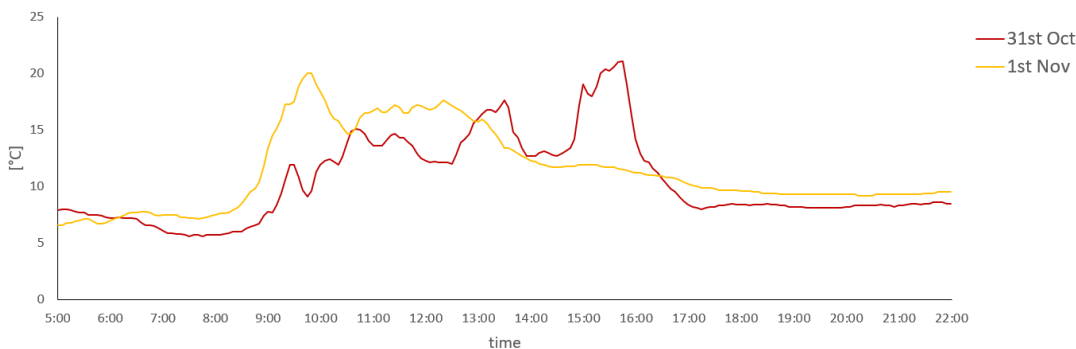
Figure 5-8: Temperature sensor measurements: air temperature

5.5.2 Data analysis real time data

Moving to Matlab for data processing operations, the initial matrixes of electrical and irradiance data were the ones already obtained and illustrated in the first approach section (namely *PPA_PV* – for electrical data, and *Pyranom* – for irradiance data), while the new temperature data were stored into two additional matrixes (one for each day: *Ta_31* – for 31st October, *Ta_01* – for 1st November). These new matrixes are schematized as follows.

Table 5-11: Ta_31 [205x2] (intervals of 5min [5:00am - 10:00pm] including data at time 0)

	Column	Column

	1	2
1. **2.**	5:00 5:05	
...	...	Air temperature 31/10 [°C]
204. **205.**	21:55 22:00	

Table 5-12: Ta_01 [205x2] (intervals of 5min [5:00am - 10:00pm], including data at time 0)

	Column 1	Column 2
1. **2.**	5:00 5:05	
...	...	Air temperature 01/11 [°C]
204. **205.**	21:55 22:00	

In contrast to the linearization case faced in the first approach section, now the sample time is regular so that the needed new data points can be obtained within the discrete set of known data points by linear interpolation. Again, given two known points represented by the coordinates (x_k, y_k) and (x_{k+1}, y_{k+1}), the new data within this range – represented by the coordinates (x_n, y_n), can be obtained through the following formula:

$$y_n = y_k + (x_n - x_k) \cdot \frac{(y_{k+1} - y_k)}{(x_{k+1} - x_k)}$$

In this case, x is the time variable t (along the x-axis) whereas y represents the temperature variable T (along the y-axis). Specifically,

$$x_{k+1} - x_k = 5min, \quad x_n = x_k + n \cdot 5\,s \qquad \text{with } n = 1, \dots, 59$$

According to this method, new data with the desired sample time of 5s were derived within each range of 5min.

Afterwards, the data within the desired 24h time frame were selected from the results of the linearization and copied into a unique matrix (named *Ta* – air temperature). The cells corresponding to the overnight missing data (from 10:00 pm to 5:00 am) have been set to 0. The resulting matrix can be schematized as follows.

Table 5-13: Ta [17281x2] (intervals of 5s within 24h, including data at time 0.)

	Column 1	Column 2
1.	Second 0	
2.	Second 5	Air temperature 31/10 [°C]
...	…	
8257.	Second 41280	---------- 0
8258.		
...	Second 41285	0 0 ----------
13296.		
13297.	…	
...	Second 66475	Air
17280.	Second 66480	temperature 11/10 [°C]
17281.		
	…	
	Second 86395	
	Second 86400	

Since, as already mentioned, the pyranometer and PPA sampling times were different from each other and also slightly imprecise, electrical variables and irradiance data processing by linear interpolation was needed. The approach followed in this case is different from the previous one and in line with the pre-processing method described in [5]. According to this reference, in fact, when input data for power system studies are provided with different time steps or even with irregular timing, a pre-processing phase is needed to unify the representation within the same time step. It is important to note that, since most of the data considered in the context of power system analysis represent the average power in a given time step, the overall energy – integral of the considered pattern over the period of interest, has to be preserved. This condition is met by introducing a correction factor calculated as follows.

For the sake of notation,

T is the total period of analysis,

τ_i is the initial irregular time step,

τ_o is the newly chosen regular time step

p_{T,τ_i} represents the vector of initial values, each with different formats and irregular time step;

$\tilde{p}_{T,\tau_o}$ represents the vector calculated from the one above on the basis of geometric considerations only (linear interpolation in this case);

p_{T,τ_o} represents the final vector of regularly distributed points at the chosen time step.

First, the total energy W_i and W_o are calculated by integrating the patterns p_{T,τ_i} and $\tilde{p}_{T,\tau_o}$, respectively, over the period T. The correction factor ξ is then calculated as the energy ratio $\xi = W_i / W_o$. At last, the final pattern is obtained through the following relation:

$$p_{T,\tau_o} = \xi \cdot \tilde{p}_{T,\tau_o}$$

In this way, the total energy of the final pattern is maintained equal to the initial one (W_i). This procedure has been followed for the patterns of active power, reactive power and irradiance. The total period of analysis is:

T = 86400 s –>   seconds in 24h

The initial vectors with irregular time steps are the columns of the initial unchanged matrixes described at the beginning of the first approach model:

$p1_{T,\tau_i}$ = *Pyranom(:,2)* -> Irradiance vector with 1441 rows – intervals of 1min within 24h, including data at time 0. Non-uniform time steps due to instrument imprecisions.

$p2_{T,\tau_i}$ = *PPA_PV(:,2)* -> PH1 active power vector with 17279 rows - intervals of 5s within 24h, including data at time 0. 2 fewer data due to instrument imprecisions.

$p3_{T,\tau_i}$ = *PPA_PV(:,3)* -> PH2 active power vector with 17279 rows.
$p4_{T,\tau_i}$ = *PPA_PV(:,4)* -> PH3 active power vector with 17279 rows.
$p5_{T,\tau_i}$ = *PPA_PV(:,5)* -> PH1 reactive power vector with 17279 rows.
$p6_{T,\tau_i}$ = *PPA_PV(:,6)* -> PH2 reactive power vector with 17279 rows.
$p7_{T,\tau_i}$ = *PPA_PV(:,7)* -> PH3 reactive power vector with 17279 rows.

The vectors with regular time steps were obtained from the ones above by linear interpolation, as calculated in the first approach to the model:

$\tilde{p}1_{T,\tau_o}$ = *Pyranom_lin(:,2)* -> irradiance vector with 17281 rows – intervals of 5s within 24h, including data at time 0. Time steps precisely equal to 5s.

$\tilde{p}2_{T,\tau_o}$ = *PPA_PV_lin(:,2)* -> PH1 active power vector with 17281 rows.
$\tilde{p}3_{T,\tau_o}$ = *PPA_PV_lin(:,3)* -> PH2 active power vector with 17281 rows.
$\tilde{p}4_{T,\tau_o}$ = *PPA_PV_lin(:,4)* -> PH3 active power vector with 17281 rows.
$\tilde{p}5_{T,\tau_o}$ = *PPA_PV_lin(:,5)* -> PH1 reactive power vector with 17281 rows.
$\tilde{p}6_{T,\tau_o}$ = *PPA_PV_lin(:,6)* -> PH2 reactive power vector with 17281 rows.
$\tilde{p}7_{T,\tau_o}$ = *PPA_PV_lin(:,7)* -> PH3 reactive power vector with 17281 rows.

The total energies W_{k_i} and W_{k_o} were calculated by integrating the patterns pk_{T,τ_i} and $\tilde{p}k_{T,\tau_o}$, respectively, over the period T^1.

T^1 In the first method this was done both by explicitly implementing the sum of trapezoidal areas underlying the patterns and by means of the Matlab function *trapz*. In details, the command T = *trapz(X,Y)* performs the trapezoidal numerical integration of Y with respect to the x-axis coordinates specified by X. Since, by comparing the results in the two cases, the difference between them ended up being every time $<10^{-7}$, the two methods were proved to be roughly equivalent. The explicit integration was at last chosen for the energy calculations.

The correction factors were then computed through the ratio $\xi k = W_{k_i}/W_{k_o}$. Finally, the final vectors with regular time steps and preserved total energy were obtained through the following formula:

$pk_{T,\tau_o} = \xi k \cdot \tilde{p}k_{T,\tau_o}$

As a final check, the total energies Wk_o' were calculated by integrating the resulting patterns pk_{T,τ_o} and compared with Wk_i. The difference $|Wk_o' - Wk_i|$ resulted $<10^{-6}$ in the worst case, so that it was possible to state that the overall energy was preserved during the processing.

At the end of the process, the resulting vectors were included in matrixes which are schematized below.

Table 5-14: PPA_PV_lin_new [17281x7]

	Column 1	Column 2	Column 3	Column 4	Column 5	Column 6	Column 7
1. 2.	Second 0 Second 5	$p2_{T,\tau_o}$ (P PH1 [W])	$p3_{T,\tau_o}$ (P PH2 [W])	$p4_{T,\tau_o}$ (P PH3 [W])	$p5_{T,\tau_o}$ (Q PH1 [var])	$p6_{T,\tau_o}$ (Q PH2 [var])	$p7_{T,\tau_o}$ (Q PH3 [var])
...	...						
17281.	Second 86400						

Table 5-15: Pyranom_lin_new [17281x2]

	Column 1	Column 2
1. 2.	Second 0 Second 5	$p1_{T,\tau_o}$ (Irradiance [W/m²])
...	...	
17281.	Second 86400	

5.6 Creation of final model.

According to the concept underlined in the introduction to this chapter, the idea of this second version was to provide as outputs the produced electrical power, both active and reactive, in order to control the dynamic load block. Moreover, as an improvement to the first model, the further idea was to take as input not only irradiance values but also temperature ones. In order to estimate the generated active power starting from irradiance and temperature inputs, the model described [6] and already used for STORE&GO project [7] was taken as reference.

This model allows the irradiance profile (G, in [W/m²]) to be converted into power – in particular, into a dimensionless value obtained through the ratio between the produced power on the AC side (P_{AC}, in [W]) and the PV plant nominal power (P_{nom}, in [W$_p$]), which represents the production profile (in [Pu_0]). The air temperature pattern (T_a, in [°C]) is used first to calculate the solar cell temperature (T_c, in [°C]) and then to estimate the over-temperature losses, represented by the thermal efficiency (η_{th}). This is used to take into account the reduction of production due to the PV panels over-temperature. The corresponding formulas are:

$$T_c = T_a + \frac{NOCT - 20}{800} \cdot G$$

$$\eta_{th} = 1 - \alpha_{th} \cdot (T_c - 25)$$

$$\frac{P_{AC}}{P_{nom}} = \eta_{DC/AC} \cdot \frac{G}{1000} \cdot \eta_{th}$$

$NOCT$ is the Nominal Operating Cell Temperature;

α_{th} is the thermal coefficient of the PV module (dependent on the PV technology);

$\eta_{DC/AC}$ is the efficiency – affected by losses due to reflection, dirt, I-V characteristic mismatch, DC cables, DC/AC conversion, tolerance and so on.

Note : G_{STC} = 1000 W/m^2 and $T_{C,STC}$ = 25 °C define the Standard Test Conditions

G_{NOCT} = 800 W/m^2 and $T_{a,NOCT}$ = 20 °C define the Nominal Operating Cell Temperature

In particular, in this context the model inputs are:

$G = Pyronom\_lin\_new(:,2)$, $T_a = Ta(:,2)$

while the model constants have been set as follows:

$NOCT$ = 44 °C   (PV module data table 5-16)
α_{th} = 0.41%/°C   (PV module data sheet table 5-16)
P_{nom} = 16 · 260 W$_p$ (16 modules, each one with nominal power of 260 W$_p$ from PV module data sheet table 5-16)
$\eta_{DC/AC}$ = 0.59   (estimated by trial, in such a way to minimize the difference between P_{AC} output pattern and the actual power profile produced by the PV plant)

The model output is resulting in a vector *Pac_fin* [17281x2] compared with the one representing the real PV panels output (*-PPA_PV(:,2)* – PH1 active power multiplied by -1 -> produced power marked as positive). The resulting graph is displayed in figure 5-9.
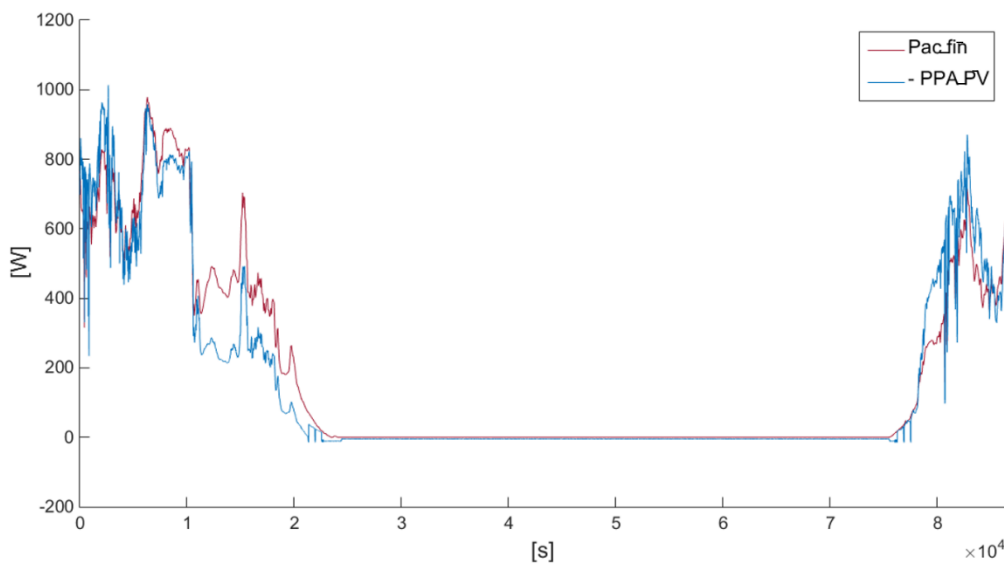
Figure 5-9: Final version of model: comparison estimated and measured active power[1]

In this way, it can be observed that the two profiles are very close to each other, so that the correctness and the accuracy of the adopted model is demonstrated.

---

[1] For this purpose only the active power of phase 1 has been considered. In fact, the active power of the other two phases, being roughly constant throughout the 24h measurements, have been proven to be constituted by electrical losses only. It means that the PV power conversion is operated only over one phase.

To conclude, it is possible to claim that the model is precise and also, what was considered the main goal, general. This means that, given a generic irradiance vector as input, the model would return a power profile acceptably similar to the real one, regardless of atmospheric conditions and time of the year.

However, the analyzed model is only able to provide the generated active power, while both active and reactive powers are needed in order to control the mentioned dynamic load block. In this regard, the developed idea has been to estimate the generated reactive power from the active one already evaluated by means of a look-up table representing the function Q(P). The procedure followed for this purpose is the one previously carried out for the first model approach. In that case, the functions to be implemented were *P(irr)* and *Q(irr)*. It follows that this time the active power vector (*PPA_PV_lin_new(:,2)* – PH1 active power) has been treated as the irradiance array (*Pyranom_lin*) and the reactive power vector (*PPA_PV_lin_new(:,5)* – PH1 reactive power) as the electrical variables matrix (*PPA_PV_lin*). Briefly, in order to make the independent variable monolithically increasing as needed, the elements of the active power vector were sorted in ascending order. The reactive power vector was then rearranged accordingly. At last, the rows corresponding to repetitive active power values was deleted from both the active and reactive power vectors. For the reactive power vector, the mean value of the set of detected rows was calculated and stored in the only cell in the group left.

The resulting arrays are:

P_lin_new_sort_del [17268x2] and *Q_lin_new_sort_del_mean* [17268x2][2]

In Figure 5-10 it can be observed the complete PV panels model. It is supplied by an ideal generator modeled through a Three-Phase Source block, while all the necessary electrical variables are measured through appropriate measurement blocks. It is worth to notice that this is only a default setup, used for the model final testing. Afterwards, the tested model can be included in a more general network simulation.
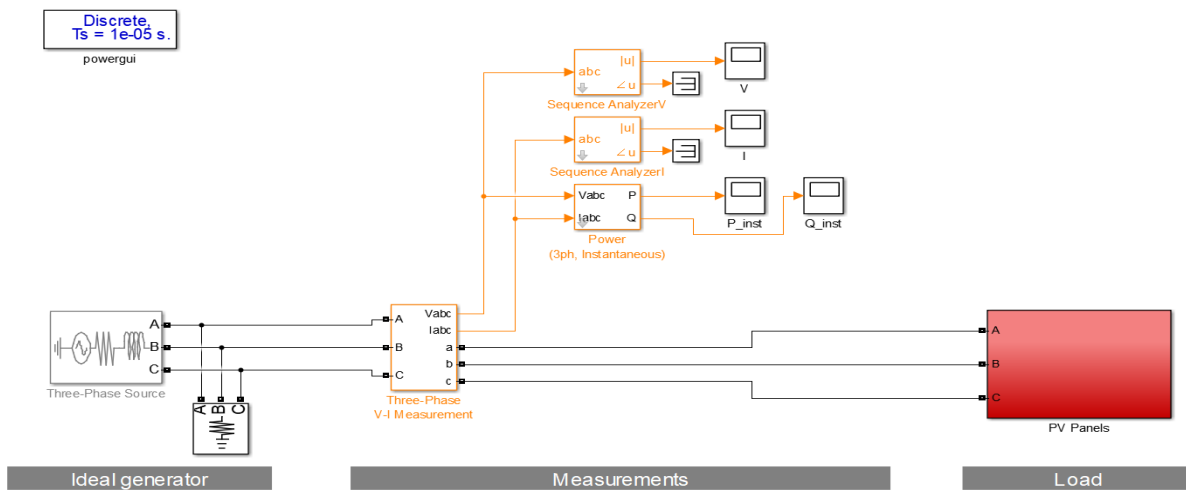

Figure 5-10: Final version of the PV panels model

Figure 5-11 shows in detail the *PV Panels* subsystem. It includes a Three-Phase Dynamic Load block whose active and reactive power are externally controlled and received from the *PV_model* subsystem. The inputs to this subsystem are the above described vectors of solar irradiance (named *Pyranom_lin_new*) and air temperature (named *Ta*) while the content of the subsystem itself is

---

[2] They can be schematized with the same logic of the previous Pyranom_lin_sort_del and PPA_PV_lin_sort_del_mean.

depicted in figure 5-11. Here the first blocks that appear on the left (indicated as *G(t)* and *Ta(t)*) have been created in order to upload subsequent cells of the array, in accordance to the clock ticks implemented by the *Counter* subsystem, in figure 5-12. The central part corresponds to the graphical implementation of the formulas analyzed above, which allows to obtain the produced active power starting from irradiance and temperature data. At last, on the right, the previously mentioned look-up table enables to pass from active to reactive power.
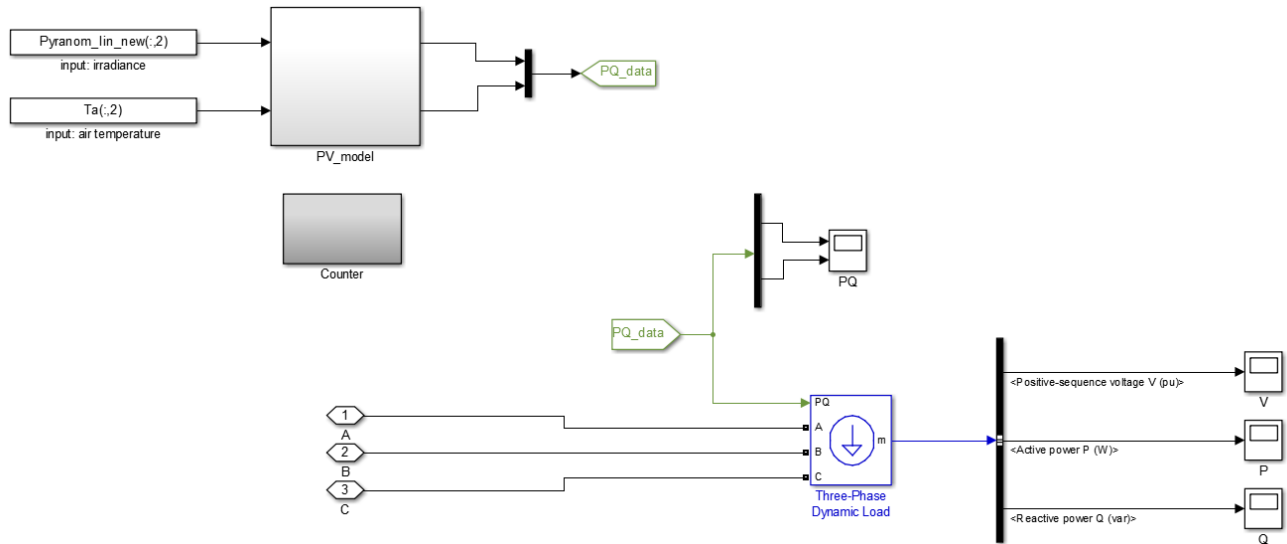

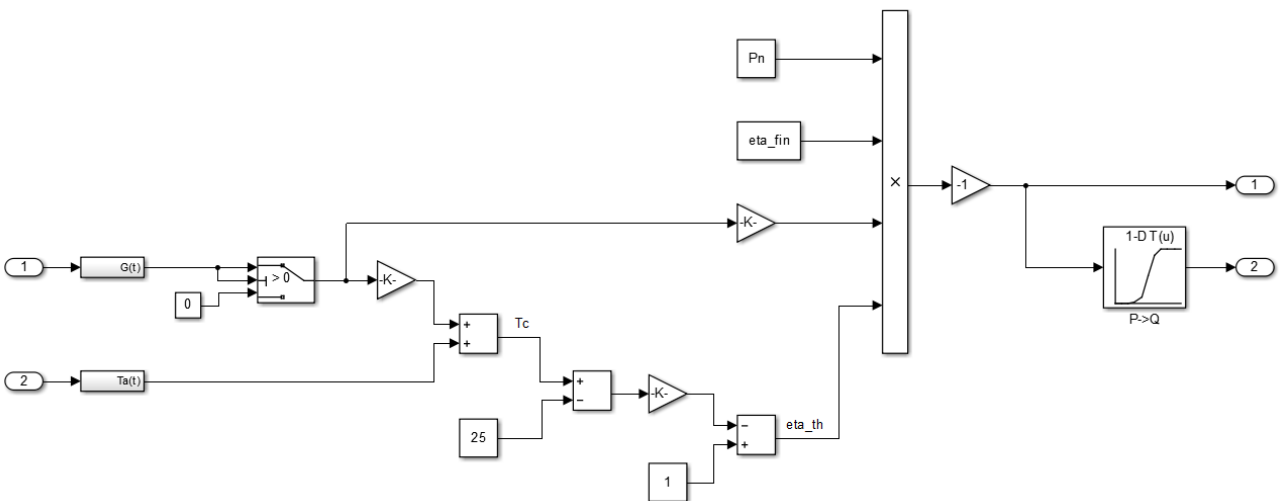**Figure 5-11:** Final version of the PV panels model: PV Panels subsystem

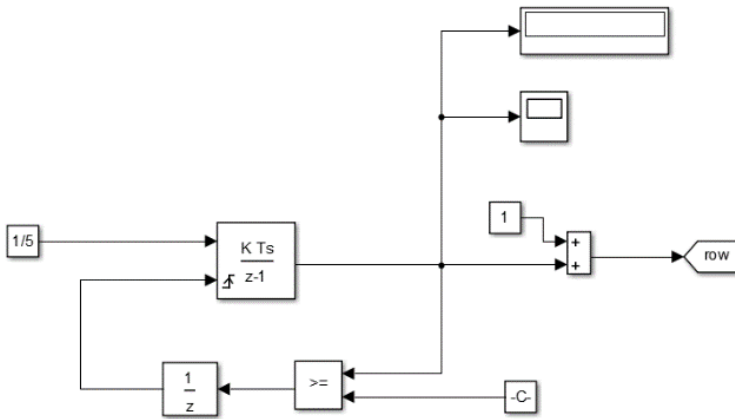**Figure 5-12:** Final version of the PV panels model: PV_model subsystem

Figure 5-13: Final version of the PV panels model: Counter subsystem

Trina solar, PV panel model TSM-260PC05A	
ELECTRICAL DATA @ STC	
Peak Power - P_{MAX} [W_p]	260
Maximum Power Voltage – V_{MPP} [V]	30.6
Maximum Power Current - I_{MPP} [A]	8.50
Open Circuit Voltage – V_{OC} [V]	38.2
Short Circuit Current – I_{SC} [A]	9.00
Module efficiency - η_m [%]	15.9
MECHANICAL DATA	
Solar cells	Multicrystalline 156 x 156 mm
Module dimensions	1650 x 992 x 35 mm
Weight	18.6 kg
TEMPERATURE RATINGS	
Nominal Operating Cell Temperature (NOCT)	44 °C ($\pm$2 °C)
Temperature Coefficient of P_{MAX}	-0.41 %/°C
Temperature Coefficient of V_{OC}	-0.32 %/°C
Temperature Coefficient of I_{SC}	0.053 %/°C
Operational Temperature	-40~+85 °C

Table 5-16: Trina solar PV panels specifications

Note: Values important for model calculations presented in the following section.

STC (Standard Test Conditions): Air Mass AM1.5. Irradiance 1000 W/m². Cell Temperature 25 °C. Power measurement tolerance: $\pm$3%

NOCT (Nominal Operating Cell Temperature): Irradiance 800 W/m². Ambient Temperature 20 °C. Wind Speed 1 m/s. Power measurement tolerance: $\pm$3%

SolarEdge, Three-phase inverter model SE4K	
OUTPUT	
Rated AC Output Power	4000 W
Maximum AC Output Power	4000 W
Nominal Operating Voltage	220/230 V_{AC} (L-N) 380/400 V_{AC} (L-L)
Maximum Output Current	6.5 A_{AC}
Nominal Operating Frequency	50/60 Hz
INPUT	
Maximum DC Power (Module STC)	5400 W
Input Voltage range	680 – 950 V_{DC}
Maximum Input Current	7 A_{DC}
Maximum Inverter Efficiency	98%
INSTALLATION SPECIFICATIONS	
Protection Rating	IP65
Installation	Indoor

Table 5-17: Solar Edge's three-phase inverter specifications

6   Matlab/Simulink static electrolyser model

Similarly to the PV panels, also the first stage of the electrolyser modelling required to perform a series of measurements, which in this case are the following:

- Electrical variables related to the electrolyser consumed AC power (upstream of the rectifier AC/DC conversion) at 25, 50, 75 and 100% of full-load by means of the PPA power analyzer
- Hydrogen production process parameters at the various percentage of the load by means of PLC and HOGEN40 software

For the purpose of characterizing the electrolyser behavior, various experiments had to be performed under various load conditions, quantified as 25, 50, 75 and 100% of full-load. The idea was to simulate the H_2 load supply by operating the electrolyser in venting mode, and, in order to achieve the reduced load operation, to properly close the valves regulating the H_2 output flow. In fact, because of the almost linear relationship, a certain percentage of the maximum hydrogen flow rate roughly corresponds to the same percentage of maximum electrical consumption. We have taken 2 series of measurements of 2h duration with 1s time step. Under each load condition, all the hydrogen production process parameters were logged by using both PLC and the electrolyser software. In all cases, the selected sampling times were the minimum handled by each method, respectively, 10s for the PLC and 5s for HOGEN40 software.

A special attention was payed to the synchronization of all measuring instruments during each performed experiment. At last, the entire set of retrieved data were imported in Excel to produce the associated graphs for data analysis.
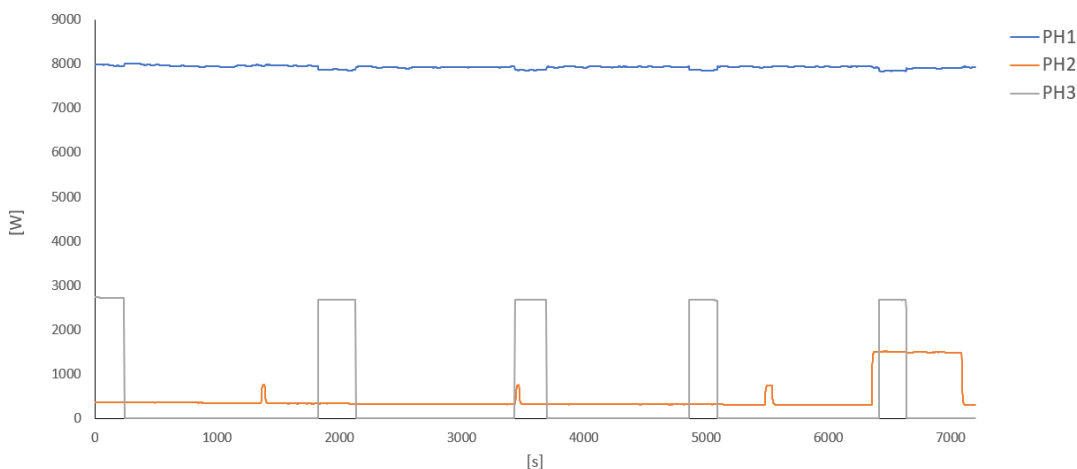

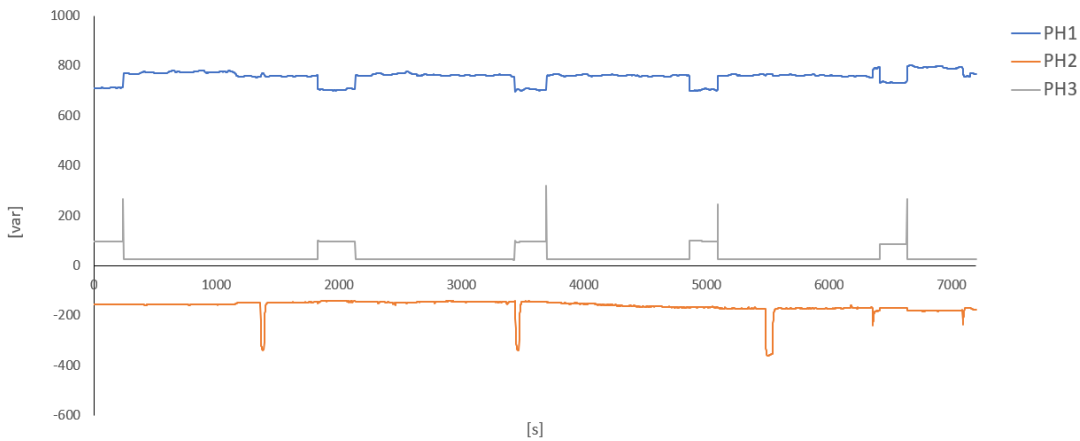**Figure 6-1:** Three-phase active power at full load

Figure 6-2: Three-phase reactive power at full load

As a comment, when analyzing the power data at 1s time step, a phase power imbalance was observed over the three phases. While the power consumption of phase 1 changes according to the load percentage, the other two phases always show roughly the same behavior independently of load conditions. This can be explained by the fact that, due to the small size of the electrolyser, the DC voltage required by the electrolysis process is rectified via a single phase only and the power consumption over phase 1 and 2 only represent power dissipation. The small dissipation is related to the electrolyser cabin lights and heating system and is constant during all the measured cycles. In addition, a huge gap in power consumption was observed between AC and DC side. This is again related to the small size of the unit and its consequent low efficiency. As an example, the most significant results of active and reactive power (on the AC side), DC power obtained by multiplying voltage and current of the stack (on the DC side) and hydrogen output flow are depicted in the following figures. Figure 6-1 and 6-2 shows active and reactive power for all three phases, with phase 2 and 3 keeping nearly the same pattern at the other load percentage as well. Figure 6-3 and 6-4 highlight the change in active and reactive power by varying the load. By comparing the H_2 output flow in figure 6-6 with the AC power in figure 6-3 the approximately linear relationship between these two quantities is demonstrated. At last, the comparison between the DC stack power in figure 6-5 and the AC power in the previous figure 6-3 shows the losses due to AC/DC conversion.
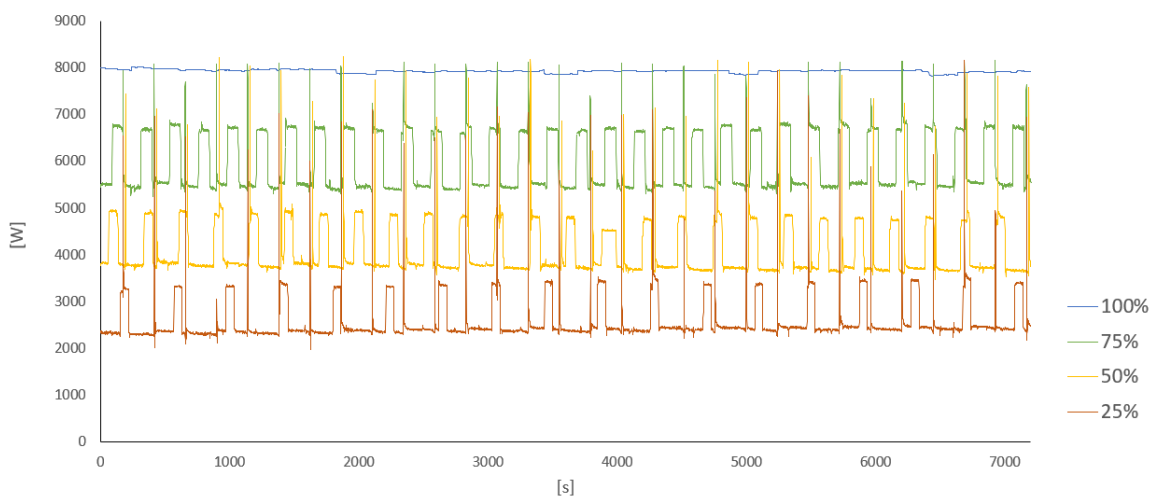

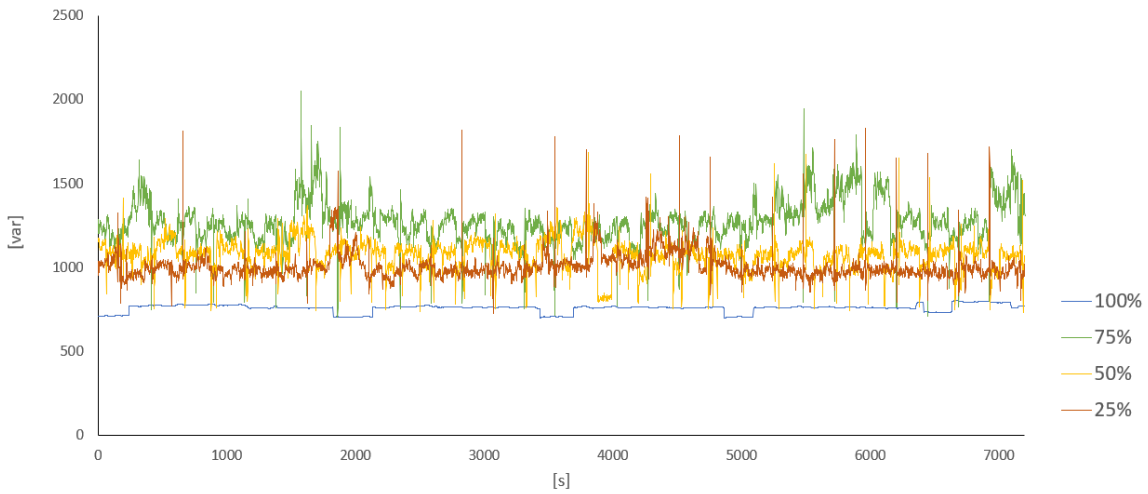**Figure 6-3:** Active power of phase 1 by varying the load

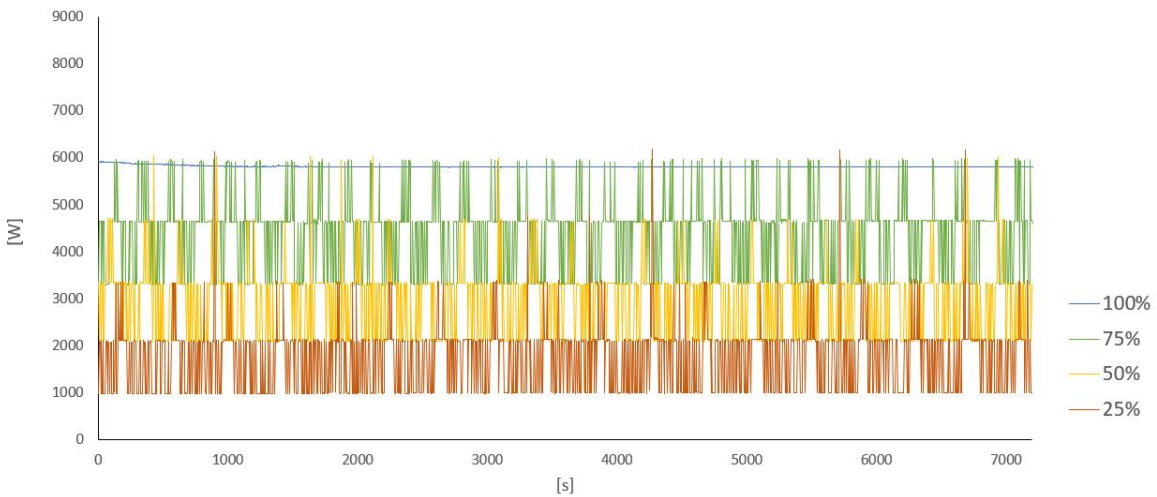**Figure 6-4:** Reactive power of phase 1 by varying the load

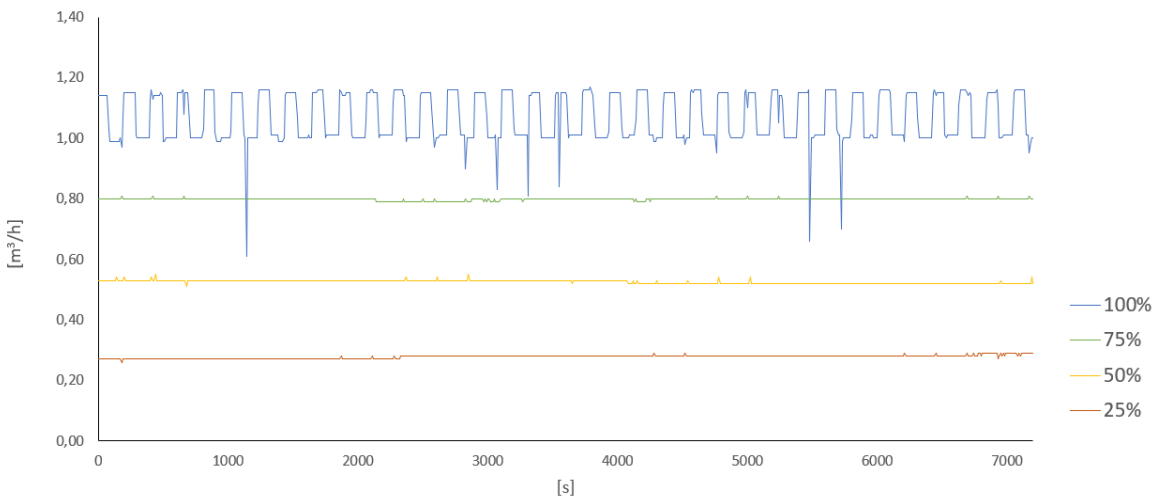**Figure 6-5:** DC power by varying the load

Figure 6-6: H_2 output flow by varying the load

At last, by analyzing the measured power at 20ms time step, the active power of phase 1 for all the partial load conditions was observed to vary with a higher frequency and within a wider range than the respective waveforms measured at 1s time step. This detail was made visible owing to the lower PPA sampling time. Such a huge and quick change in power consumption is due to the converter switching. As an illustration, Figure 6-7 shows the active power for all three phases retrieved during the 20ms time step experiment at 25% of full-load. What said is proven by comparing these waveforms with the ones in figure 6-8, representing the three-phase active power at the same percentage of full-load but measured during the 1s time step experiment. Finally, the comparison of the corresponding three-phase reactive power is possible by observing figure 6-9 and 6-10.
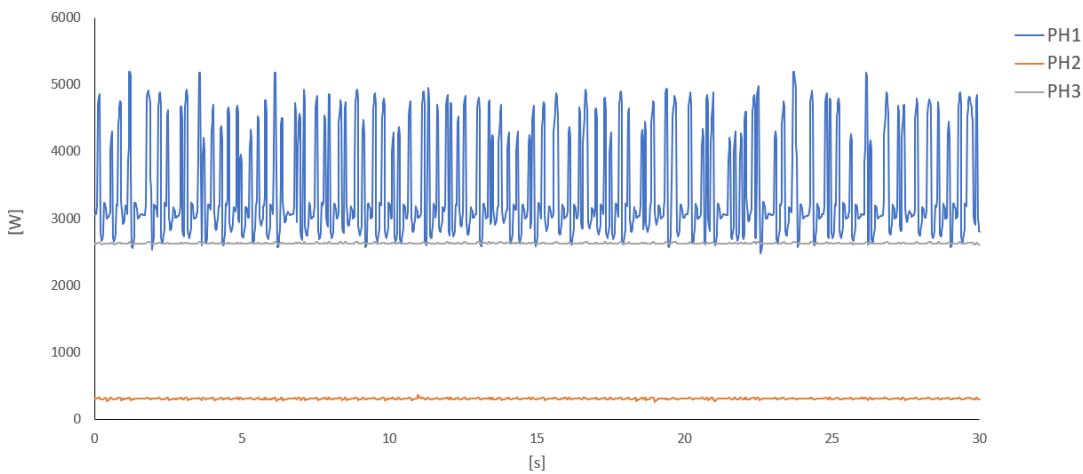

Figure 6-7: Three-phase active power at 25% of full-load and time step of 20ms
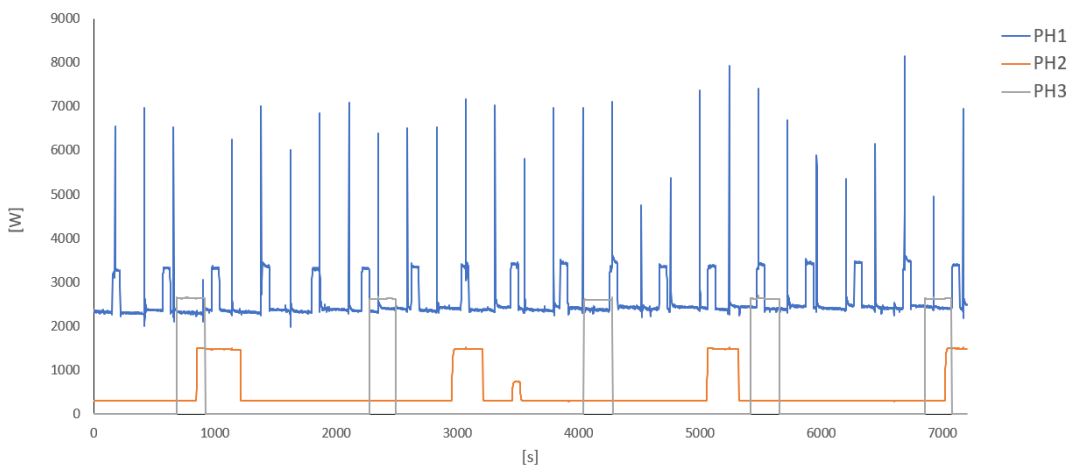
Figure 6-8: Three-phase active power at 25% of full-load and time step of 1s
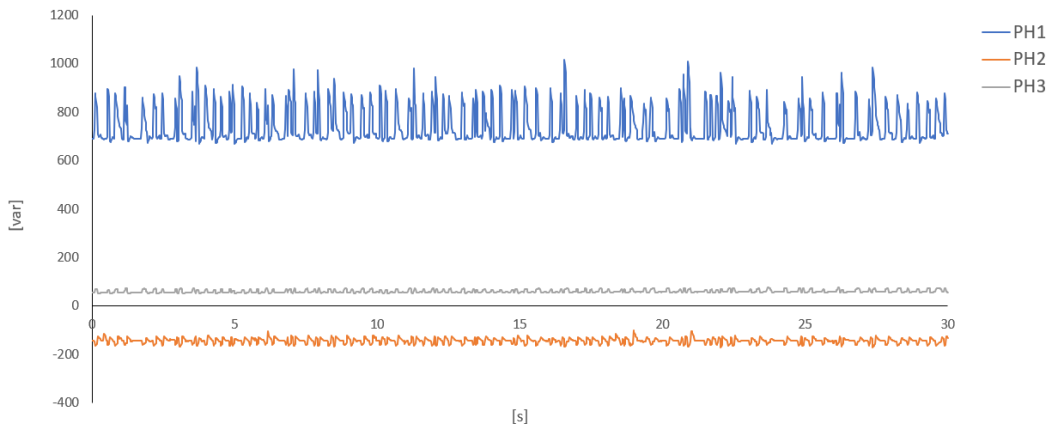
Figure 6-9: Three-phase reactive power at 25% of full-load and time step of 20ms
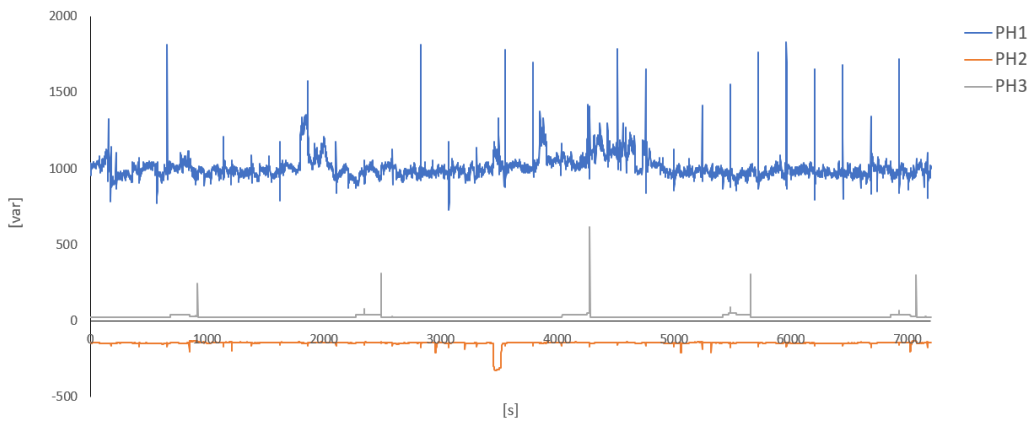
Figure 6-10: Three-phase reactive power at 25% of full-load and time step of 1s

6.1   Matrixes Definition and linearization

After both the measurements of 2h and 30s duration, the collected electrical data of active and reactive power were imported to Matlab for data processing operations and stored into eight matrixes (four matrixes for each experiment and one matrix for each percentage of full-load production.

Specifically, these are: *PQ_x_2h*, where *x = 25, 50, 75, Full* – P and Q at 25, 50, 75, 100% of full-load for the experiment of 2h duration; *PQ_x*, where *x = 25, 50, 75, Full* – P and Q at 25, 50, 75, 100% of full-load for the experiment of 30s duration).

As an example, a graphical representation of the matrix columns is provided as follows.

Table 6-1: PQ_25_2h [6910x7] (intervals of roughly 1s within 2h)

	Column 1	Column 2	Column 3	Column 4	Column 5	Column 6	Column 7
	Seconds from 0	P PH1 [W]	P PH2 [W]	P PH3 [W]	Q PH1 [var]	Q PH2 [var]	Q PH3 [var]
1.	Second 0						
2.	Second 2.002						
3.	Second 3						
...	...						
6909.	Second 7199.3						
6910.	Second 7200.3						

Table 6-2: PQ_25 [1501x7] (intervals of roughly 20ms within 30s)

	Column 1	Column 2	Column 3	Column 4	Column 5	Column 6	Column 7
	Seconds from 0	P PH1 [W]	P PH2 [W]	P PH3 [W]	Q PH1 [var]	Q PH2 [var]	Q PH3 [var]
1.	Second 0				Calculated from the PPA measured data through the formula: $Q_{abs,n} = \sqrt{S_n^2 - P_n^2}$, where $n = 1,2,3$* Then $Q_1 = Q_{abs,1}$, $Q_2 = -Q_{abs,2}$, $Q_3 = Q_{abs,3}$		
2.	Second 0.021						
3.	Second 0.041						
...	...						
1501.	Second 30						

Note : The PPA does not measure reactive power in high-speed mode

This schematic illustration is also representative of the other collected matrixes. Briefly, the instrument sampling time appeared to be non-regular over the measured intervals, leading to fewer data than expected. It was then necessary to uniform the time step of all matrixes and, in order to do so, the same procedure of linear interpolation and extrapolation applied in the PV panels section was used. As a result, a uniform time step of 20ms was obtained for the electrical variables measured during the 2h duration and 30s duration experiments. (In particular, the matrixes are identified as *PQ_x_2h20ms_lin*, where *x = 25, 50, 75, Full* – for the experiment of 2h duration, *PQ_x_lin*, where *x = 25, 50, 75, Full* – for the experiment of 2h duration). An exemplification of the result at 25% of full-load is given below.

Table 6-3: PQ_25_2h20ms_lin [360001x7] (intervals of 20ms within 2h, including data at time 0)

	Column 1	Column 2	Column 3	Column 4	Column 5	Column 6	Column 7
1.	Second 0	P PH1 [W]	P PH2 [W]	P PH3 [W]	Q PH1 [var]	Q PH2 [var]	Q PH3 [var]
2.	Second 0.02						
3.	Second 0.04						
...	...						
360001.	Second 7200						

Table 6-4: PQ_25_lin [1501x7] (intervals of 20ms within 30s, including data at time 0.)

	Column 1	Column 2	Column 3	Column 4	Column 5	Column 6	Column 7
1.	Second 0	P PH1 [W]	P PH2 [W]	P PH3 [W]	Q PH1 [var]	Q PH2 [var]	Q PH3 [var]
2.	Second 0.02						
3.	Second 0.04						
...	...						
1501.	Second 30						

At this point, according to [5], the process unification of data within the same time step required a further operation to maintain the total energy of the final pattern equal to the initial one. This method has been already illustrated as part of the PV panels modelling. The same formulas were applied in this case to all the eight matrixes of active and reactive power. By reminding the already given notation, an exemplification of the procedure carried out for the 2h experiment is presented below:

T represents the total period of analysis, equal to: T = 2 h = 7200 s

p_{T,τ_i} represents the vector of initial values, each one with different size and irregular time step,

$p1_{2h,\tau_i}$ = *PQ_25_2h(:,2)* -> PH1 active power
$p2_{2h,\tau_i}$ = *PQ_25_2h(:,3)* -> PH2 active power
$p3_{2h,\tau_i}$ = *PQ_25_2h(:,4)* -> PH3 active power
$p4_{2h,\tau_i}$ = *PQ_25_2h(:,5)* -> PH1 reactive power
$p5_{2h,\tau_i}$ = *PQ_25_2h(:,6)* -> PH2 reactive power
$p6_{2h,\tau_i}$ = *PQ_25_2h(:,7)* -> PH3 reactive power

All vectors with 6910 rows and non-uniform time step.

$\tilde{p}_{T,\tau_o}$ represents the vector calculated from the one above on the base of geometric considerations only (linear interpolation in this case), so:

$\tilde{p}1_{2h,\tau_o}$ = *PQ_25_2h20ms_lin(:,2)* -> PH1 active power
$\tilde{p}2_{2h,\tau_o}$ = *PQ_25_2h20ms_lin(:,3)* -> PH2 active power
$\tilde{p}3_{2h,\tau_o}$ = *PQ_25_2h20ms_lin(:,4)* -> PH3 active power
$\tilde{p}4_{2h,\tau_o}$ = *PQ_25_2h20ms_lin(:,5)* -> PH1 reactive power
$\tilde{p}5_{2h,\tau_o}$ = *PQ_25_2h20ms_lin(:,6)* -> PH2 reactive power
$\tilde{p}6_{2h,\tau_o}$ = *PQ_25_2h20ms_lin(:,7)* -> PH3 reactive power

All vectors with 360001 rows and time step precisely equal to 20ms.
The total energies Wk_i and Wk_o were calculated by respectively integrating the patterns pk_{2h,τ_i} and $\tilde{p}k_{2h,\tau_o}$ over the period T[1].

T[1] This calculation was implemented by means of the Matlab function *trapz(X,Y)*, where x is the time base, represented by the vector *PQ_25_2h(:,1)* when integrating pk_{2h,τ_i} and *PQ_25_2h20ms_lin(:,1)* when integrating $\tilde{p}k_{2h,\tau_o}$.

The correction factors were then obtained through the ratio $\xi k = Wk_i / Wk_o$. At last, the final vectors with regular time step of 1s and conserved overall energy were computed through the following formula:

$$pk_{T,\tau_o} = \xi k \cdot \tilde{p}k_{T,\tau_o}$$

The final test was carried out by the integration of the new patterns pk_{T,τ_o} and the comparison of the resulting total energies Wk_o' with the initial energies Wk_i. Since the maximum difference $|Wk_o' - Wk_i|$ turned out to be $<10^{-9}$, it was proven that the overall energy was preserved throughout the processing.

The same procedure was applied also to the 30s patterns for all the load operating conditions. At the end of the process, the resulting vectors were stored in matrixes (named *PQ_x_2h20ms_lin_new*, where *x = 25, 50, 75, Full* – for the experiment of 2h duration,

PQ_x_lin_new, where *x = 25, 50, 75, Full* – for the experiment of 2h duration). A schematic example of a matrix for the 25% case and both 2h and 30s experiments is given below.

Table 6-5: PQ_25_2h20ms_lin_new [360001x7]

	Column 1	Column 2	Column 3	Column 4	Column 5	Column 6	Column 7
1. 2. ... 360001.	Second 0 Second 0.02 ... Second 7200	$p1_{2h,\tau_o}$ (P PH1 [W])	$p2_{2h,\tau_o}$ (P PH2 [W])	$p3_{2h,\tau_o}$ (P PH3 [W])	$p4_{2h,\tau_o}$ (Q PH1 [var])	$p5_{2h,\tau_o}$ (Q PH2 [var])	$p6_{2h,\tau_o}$ (Q PH3 [var])

Table 6-6: PQ_25_lin_new [1501x7]

	Column 1	Column 2	Column 3	Column 4	Column 5	Column 6	Column 7
1. 2. ... 1501.	Second 0 Second 0.02 ... Second 1500	$p1_{30s,\tau_o}$ (P PH1 [W])	$p2_{30s,\tau_o}$ (P PH2 [W])	$p3_{30s,\tau_o}$ (P PH3 [W])	$p4_{30s,\tau_o}$ (Q PH1 [var])	$p5_{30s,\tau_o}$ (Q PH2 [var])	$p6_{30s,\tau_o}$ (Q PH3 [var])

At this point, for each load operating condition two matrixes uniformed within the same time step of 20ms are available:

PQ_x_2h20ms_lin_new, where *x = 25, 50, 75, Full* – with an overall duration of 2h (360001 values) and with a lower resolution since the data were acquired by using a 1s sampling time.

PQ_x_lin_new, where *x = 25, 50, 75, Full* – with an overall duration of 30s (1501 values) and with a very high resolution since the data were acquired by means of sampling time of 20ms. A picture for the 25% case is given in figure 6-8.

As an illustration, the patter for all three phases active power in the 25% case are still the ones shown in figure 6-9 and 6-10.

In order to get final patterns with the highest possible duration and resolution, the idea was then to overlay these two waveforms by treating the former as the mean value and the latter as the harmonic component. In details, the process consisted in: averaging the 30s vector and subtracting the obtained mean value to the 30s waveform, replicating this pattern multiple times to fit the length of the 2h waveform, adding the resulting pattern to the 2h waveform*.

* This was done for both active and reactive power, for all three phases and every loading condition and the results were stored into four new matrixes (one for each percentage of full-load, namely *PQ_x_compl*, where *x = 25, 50, 75, Full*).

For the sake of consistency, the representation of the resulting active and reactive power of ph1 at 25% of full-load is provided in figure 6-11. From this graph, it is possible to see that the mean value of the final pattern follows the initial 2h waveform (figure 6-12), while, by zooming in, the 30s waveform behaviors found.
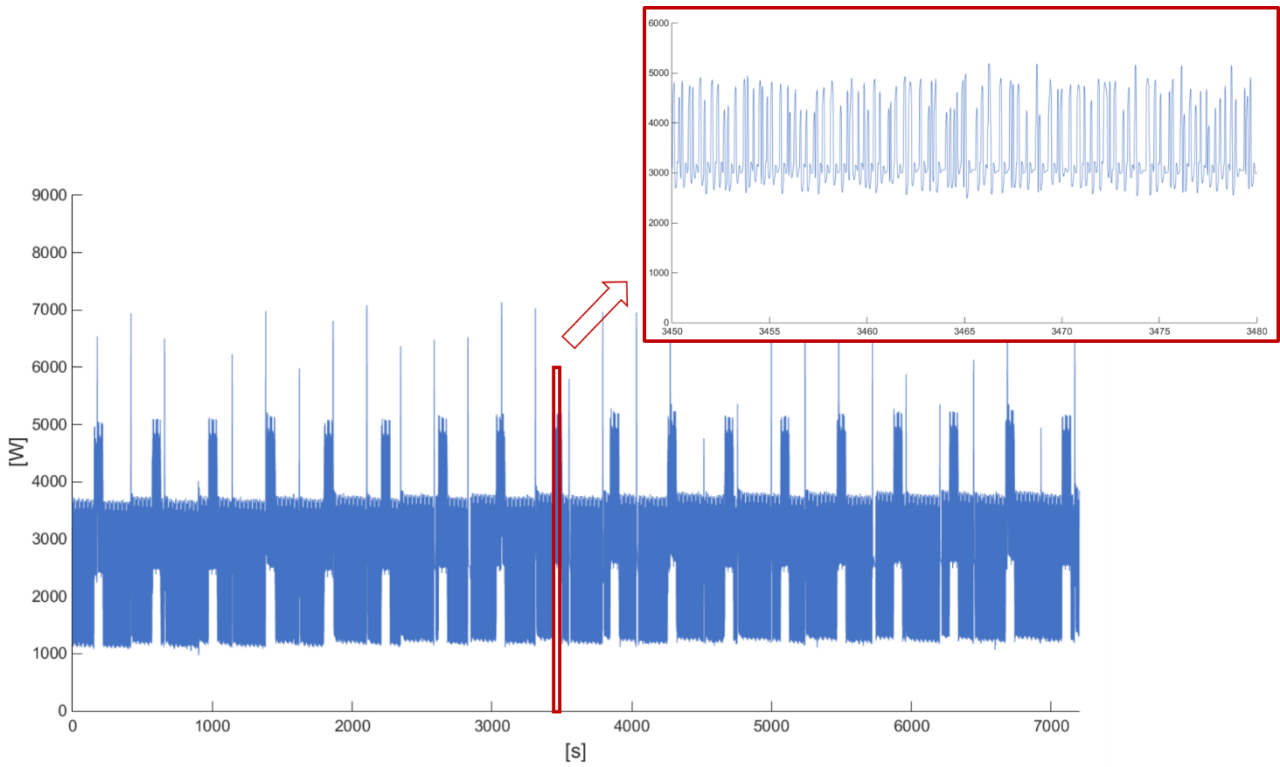
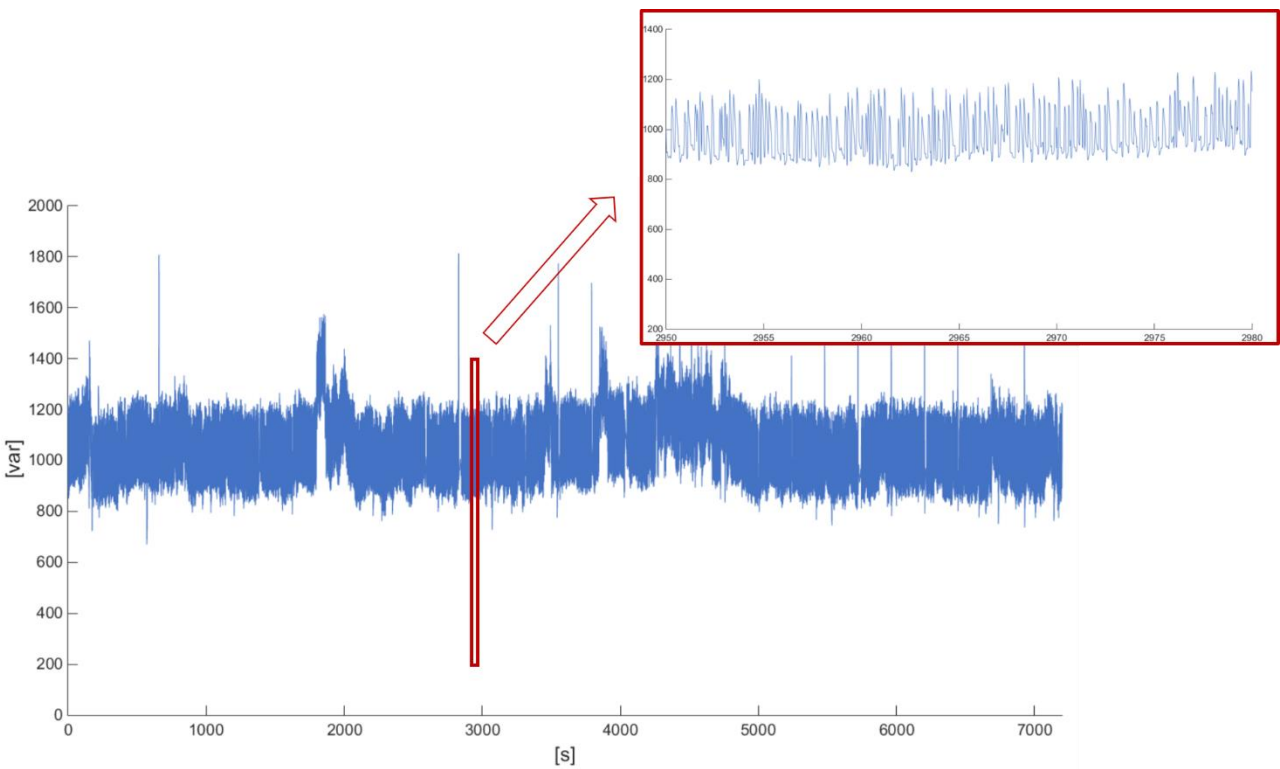**Figure 6-11:** Active power of phase 1 at 25% of full-load after overlaying process (with zoom)

Figure 6-12: Reactive power of phase 1 at 25% of full-load after overlaying process (with zoom)

A major issue in this process was that, what was indicated as the mean value (2h waveform) appeared to have a squared waveform trend (figure 6.11) , while the so-called harmonic component

(30s waveform) appeared to variate within a different range whether it was captured on the lower or higher part of the pattern. In order to obtain the most precise possible final result, it was then necessary to divide the 2h waveform into higher and lower parts and pay attention in overlaying the corresponding 20ms waveform.

The final step of the data-processing was to make sure that the total energy of the newly obtained patterns preserved the total energy of the real measured ones. Once again, this operation was carried out with reference to the formulas in [5] and reported in the PV panels section. As an example, the calculation performed for the patterns at 25% of full-load is shown below by using the well-known notation:

The total period of analysis is:

T = 2h = 7200 s

The initial vectors with irregular time steps are still represented by the real measured data:

$p1_{2h,\tau_i}$ = *PQ_25_2h(:,2)* -> PH1 active power
$p2_{2h,\tau_i}$ = *PQ_25_2h(:,3)* -> PH2 active power
$p3_{2h,\tau_i}$ = *PQ_25_2h(:,4)* -> PH3 active power
$p4_{2h,\tau_i}$ = *PQ_25_2h(:,5)* -> PH1 reactive power
$p5_{2h,\tau_i}$ = *PQ_25_2h(:,6)* -> PH2 reactive power
$p6_{2h,\tau_i}$ = *PQ_25_2h(:,7)* -> PH3 reactive power

The vectors with regular time steps obtained from the ones above by geometric considerations (overlaying of waveforms) are the columns of the newly obtained matrixes:

$\tilde{p}1_{2h,\tau_o}$ = *PQ_25_compl(:,2)* -> PH1 active power
$\tilde{p}2_{2h,\tau_o}$ = *PQ_25_compl(:,3)* -> PH2 active power
$\tilde{p}3_{2h,\tau_o}$ = *PQ_25_compl(:,4)* -> PH3 active power
$\tilde{p}4_{2h,\tau_o}$ = *PQ_25_compl(:,5)* -> PH1 reactive power
$\tilde{p}5_{2h,\tau_o}$ = *PQ_25_compl(:,6)* -> PH2 reactive power
$\tilde{p}6_{2h,\tau_o}$ = *PQ_25_compl(:,7)* -> PH3 reactive power

As done before, the total energies Wk_i and Wk_o corresponding to the integral of the patterns pk_{T,τ_i} and $\tilde{p}k_{T,\tau_o}$ over the period T were calculated , as well as the correction factor $\xi k = Wk_i/Wk_o$.

The calculation was also implemented by using the Matlab function *trapz(X,Y),* where x is the time vector, thus *PQ_25_2h(:,1)* for pk_{2h,τ_i} and still *PQ_25_2h20ms_lin(:,1)* for $\tilde{p}k_{2h,\tau_o}$.

Finally, the ultimate vectors with preserved overall energy were computed through the well-known formula:

$$pk_{T,\tau_o} = \xi k \cdot \tilde{p}k_{T,\tau_o}$$

The final check consisting in the comparison $|Wk_o' - Wk_i|$ between the total energy Wk_o' resulting from the patterns pk_{T,τ_o} and the known Wk_i resulted <10[-9] in the worst case, which means that overall energy was actually preserved throughout the entire processing.

As the ultimate step, the resulting vectors were included in the final matrixes (one for each loading condition, namely *PQ_x_compl_new*, where *x* = 25, 50, 75, Full). The matrix for the 25% case is schematized below.

Table 6-7: PQ_25_compl_new [360001x7]

	Column 1	Column 2	Column 3	Column 4	Column 5	Column 6	Column 7
1.	Second 0	$p1_{2h,\tau_o}$	$p2_{2h,\tau_o}$	$p3_{2h,\tau_o}$	$p4_{2h,\tau_o}$	$p5_{2h,\tau_o}$	$p6_{2h,\tau_o}$
2.	Second 0.02						
		(P PH1 [W])	(P PH2 [W])	(P PH3 [W])	(Q PH1 [var])	(Q PH2 [var])	(Q PH3 [var])
...	...						
360001.	Second 7200						

Lastly, for all the analyzed load conditions, the patterns of active and reactive power of phase 1 resulting from the entire data-processing operation are depicted in figure 6-13 and 6-14 These are much more accurate if compared with the above figure 6-3 and 6-4.
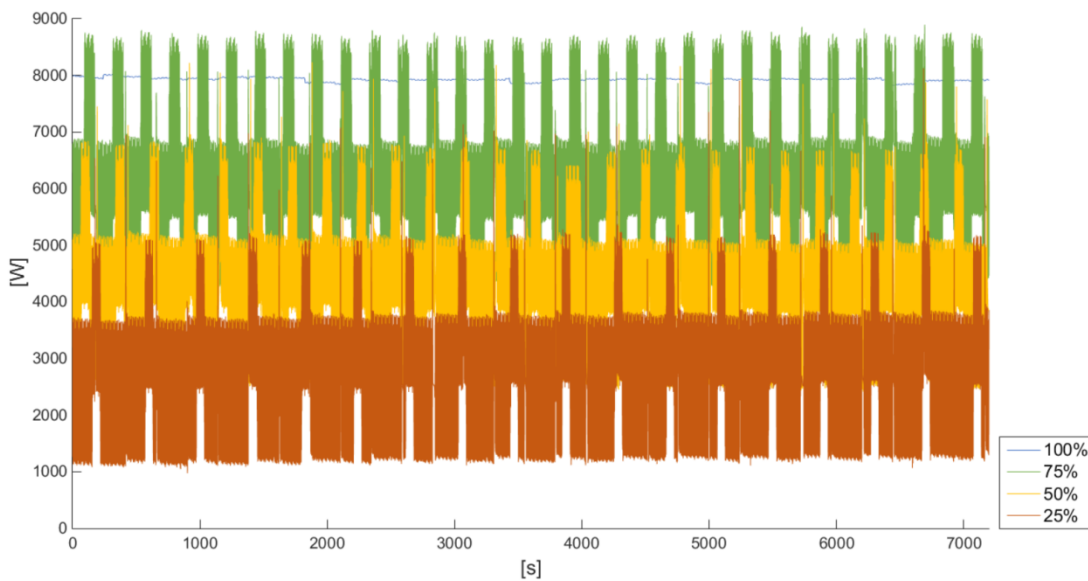

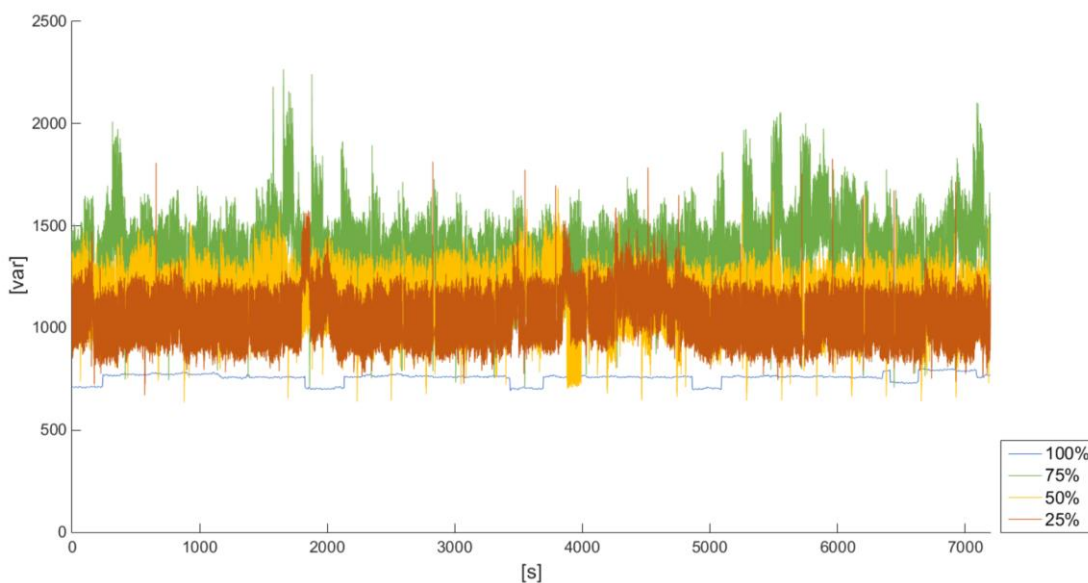**Figure 6-13:** Result of the data-processing: active power of phase 1 by varying the load

Figure 6-14: Result of the data-processing: reactive power of phase 1 by varying the load

6.2   Creation of the model

By referring back to the concept presented in the introduction to this chapter, the idea behind the measuring and following data-processing was to provide both active and reactive power consumed at different loading conditions to be given as input to the Dynamic Load block. This block along with the processed power profiles were included in the complete Electrolyser model, which is depicted in figure 6-15.
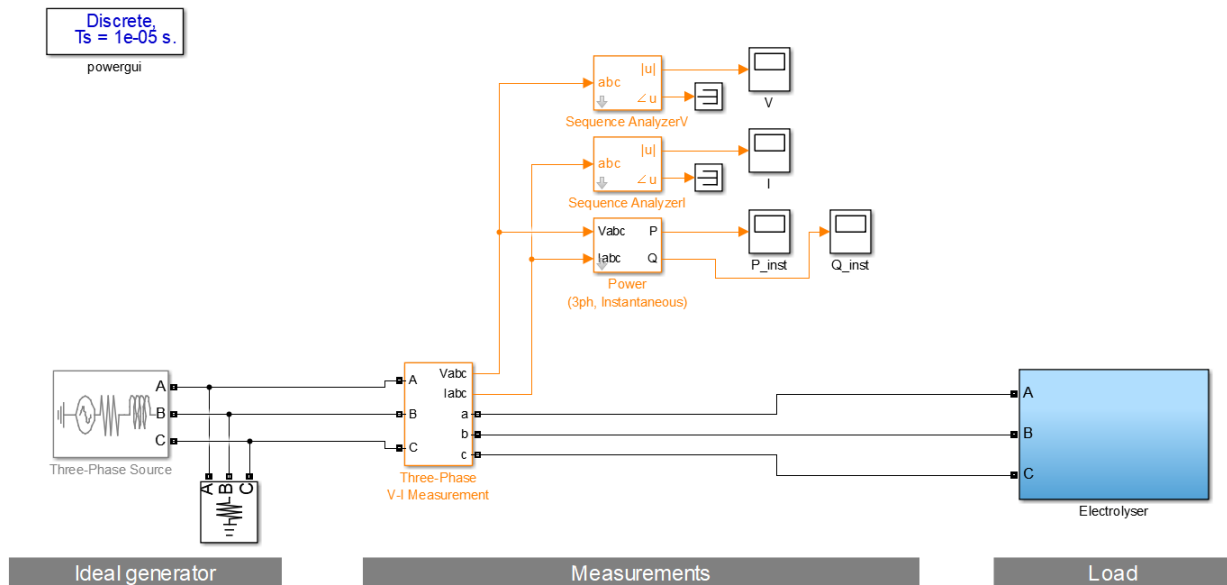

Figure 6-15: Electrolyser model

This view is conceptually similar to the one of the already illustrated PV panels model. An ideal generator modeled through a Three-Phase Source block simulates the power supply and proper measuring blocks monitor all the needed electrical variables. Once again, this only represents a basic test setup after which the model can be added to a grid simulation of desired complexity.

Figure 6-15 shows in detail the *Electrolyser* subsystem. It contains a Three-Phase Dynamic Load block whose active and reactive power are externally controlled and received from the set of blocks on the left side. This group is formed by four subsystems, one for each percentage of full-load, all with identical layout exemplified by the 25% case in figure 6-16. Here the subsystem *electrical data_25* contains the columns of the above described matrixes of active and reactive power (named *PQ_x_compl_new*, where $x = 25, 50, 75,$ Full) in the form of constant vectors. The following blocks (indicated with *f(t)*) are aimed at uploading subsequent cells of the arrays in synchrony with the clock implemented by the *Counter* subsystem. This has been already shown in the previous figure 6-16. The total active and reactive powers are then calculated by summing the values over the three phases at each time step. Moving back to the top view of figure 6-17, a multi-port switch and a constant block allow to select the desired electrolyser load. The constant block can eventually be substituted with the desired control signal.

In addition, some useful H_2 production process data have been included in the model as well. These are the profiles measured during the explained stage of data retrieving, further processed just with the purpose of unification within the chosen simulation time step of 20ms. Specifically, the H_2 flow profile can be used in case the H_2 production at the current loading condition is needed, while the stack voltage and current profiles, if multiplied, can be used to monitor the power consumption on the DC side.
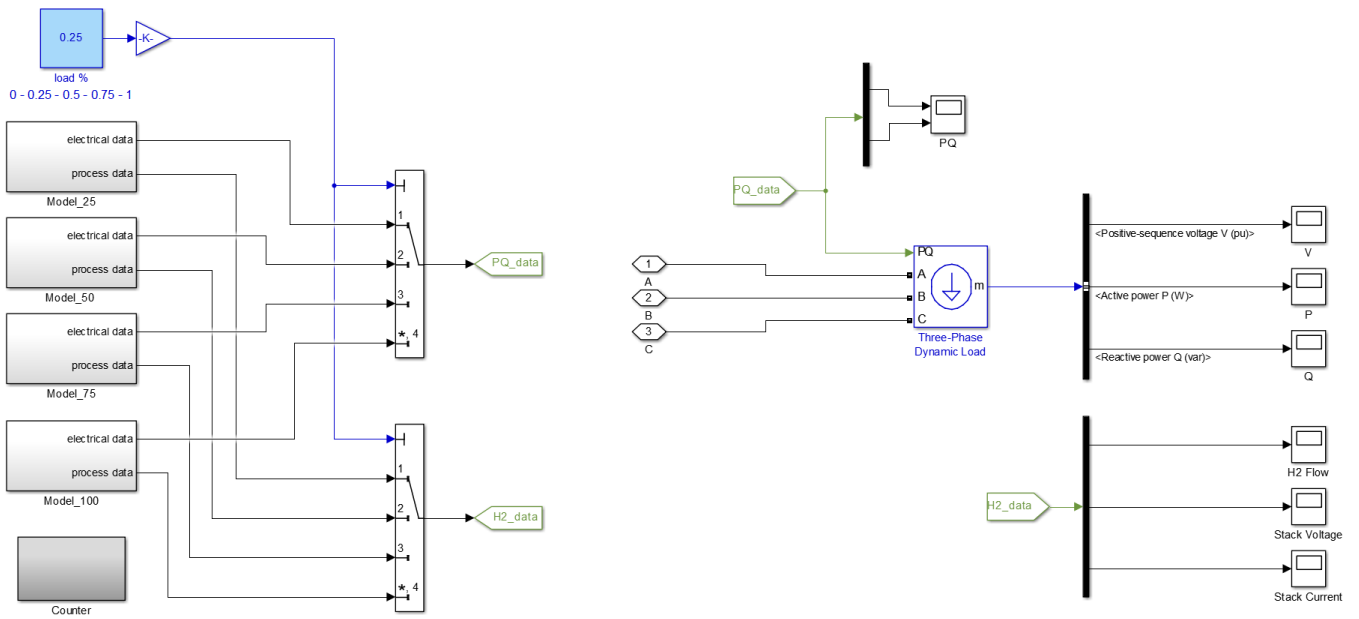
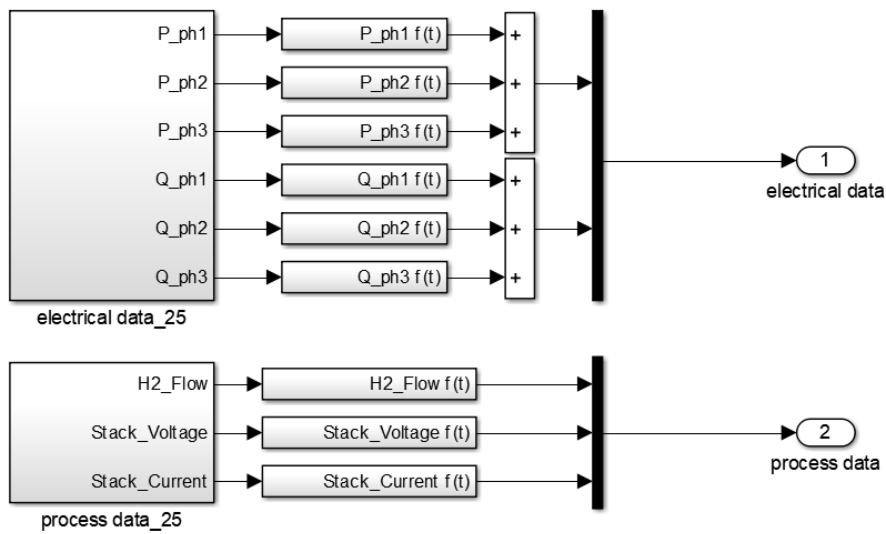**Figure 6-16:** Electrolyser model: Electrolyser subsystem

Figure 6-17: Electrolyser model: electrical data_25 subsystem

7 Matlab/Simulink dynamic electrolyser mode

In order to improve this static model, a second approach was intended to investigate the electrolyser dynamics. The dynamic interaction with is realized by the installation of a flow controller which is regulating the output flow. In fact, as confirmed during the first series of experiments, the hydrogen production rate can be considered proportional to the electrical current of the stack, this affecting the overall electrical consumption of the unit. It follows that a step change in the setpoint of hydrogen output flow produces a sudden and roughly proportional change of AC power consumption of the entire system. The parameters measured and logged:

- Control and measurement of the output hydrogen flow rate to realize step changes in the range 0–25%, 25–50%, 50–75%, 75–100% of full-load by means of the flow controller
- Measurement of the electrical variables related to the electrolyser consumed AC power (upstream of the rectifier – AC/DC conversion) during the step changes by means of the PPA power analyzer
- Measurement of the hydrogen production process parameters during the step changes by means of PLC and HOGEN40 software

As usual, great care was taken in synchronizing all measuring devices during each performed experiment. Finally, the entire set of retrieved data were imported in Excel to produce the associated graphs for data analysis. The results of all four dynamic experiments can be commented by looking at the graphs of three-phase active power and focusing on phase 1, which has been already said to be the most important phase as the one used for rectifying the DC voltage.

From the graph of the 0-25% experiment shown in figure 7-1, it is possible to observe the electrolyser start-up. In particular, the various operating states described in Chap.3.4 are visible: the first part with a low power consumption of around 400 W corresponds to the generating-vent mode; then full power of 8 kW is applied to the stack in order to build up system pressure in correspondence of the pressurize storage state. At last, after the start-up phase, the power consumption drops and the steady state at 25% of full-load is reached almost instantaneously. In this state, the power variates within a wide range around a mean value roughly equal to 25% of the maximum power (about 8 kW). This is made clear by plotting in the same graph the setpoint given to the flow controller, converted from percentage of full H_2 flow rate to percentage of full AC power consumption.
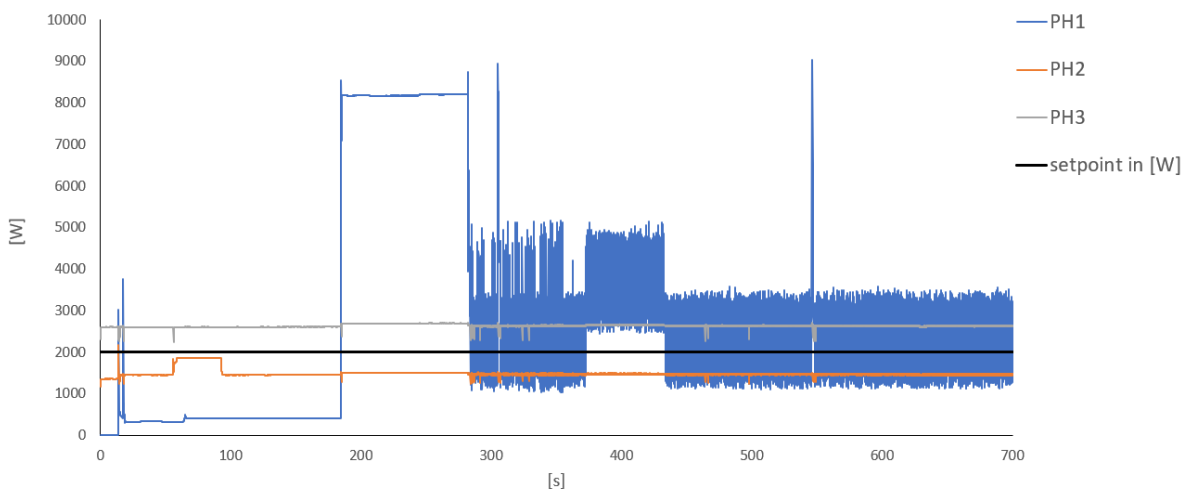

Figure 7-1: Active power of phase 1, 2 and 3 – start-up and step to 25% of full-load

From the graph of the 25-50% experiment presented in figure 7-2, it is possible to see a sudden change from the steady state at 25% of full-load to the next steady state at 50% of full-load, both marked by the variation of power consumption around the line which represents the setpoint.
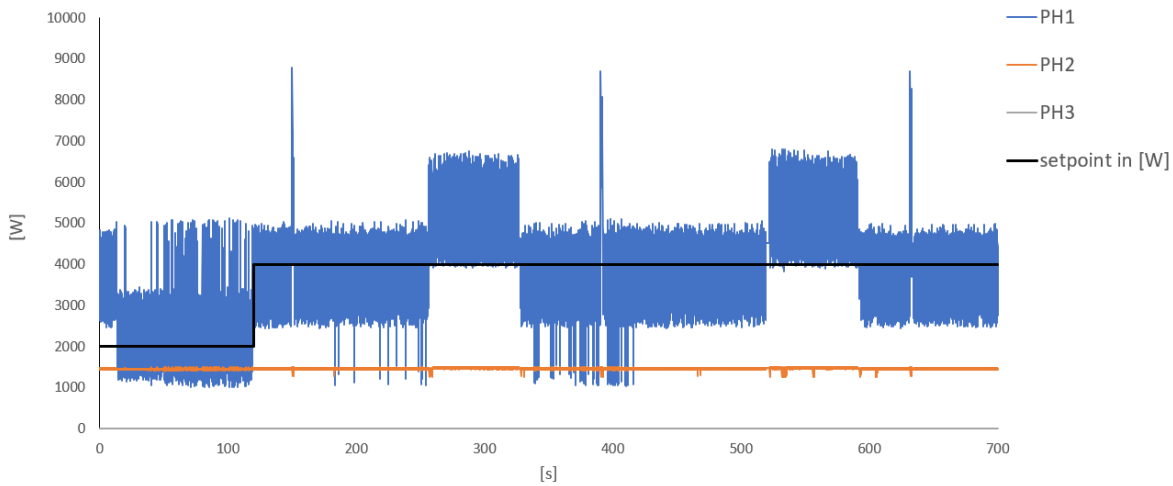

Figure 7-2: Active power of phase 1, 2 and 3 – step from 25 to 50% of full-load

The same behavior can be inferred also from the 50-75% and 75-100% experiments, whose graphs are shown in figure 7-3 and 7-4. Basically, at a certain percentage of full H_2 flow rate the active power variates approximately around the same percentage of maximum power consumption. Only at full H_2 flow rate the power is roughly constant and exactly equal to the maximum power consumption. In any case, the dynamic of the change from one steady state to another is almost absent.
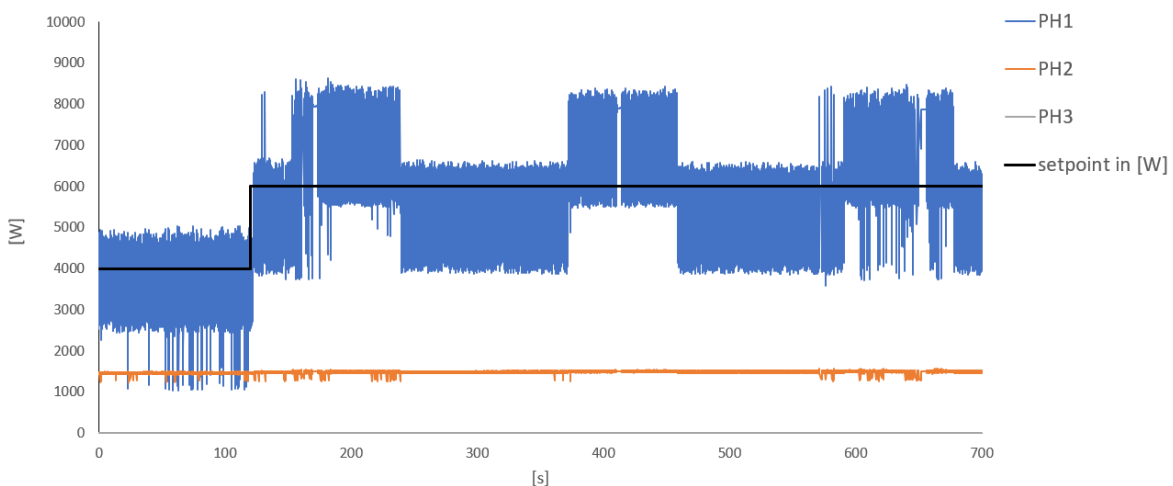

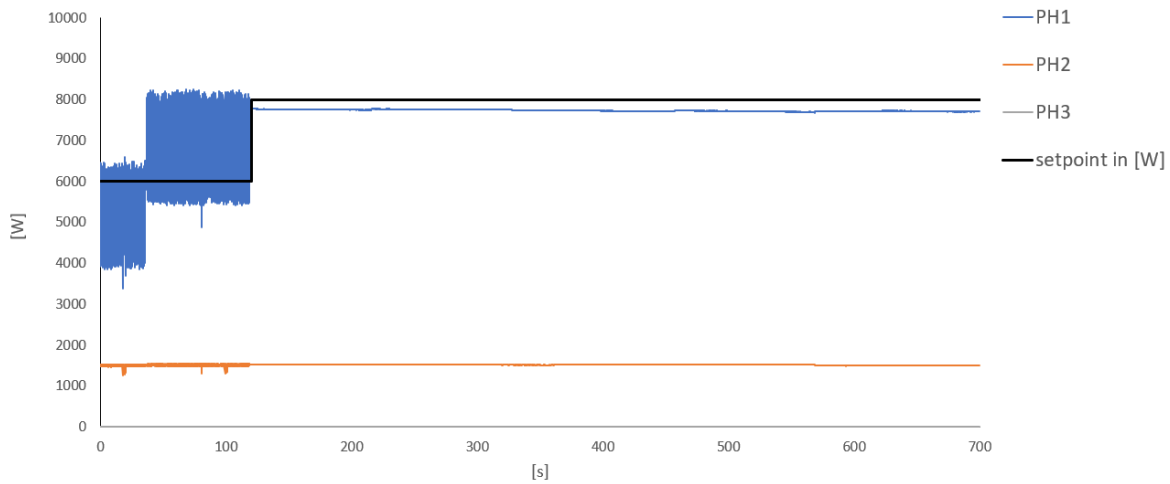**Figure 7-3:** Active power of phase 1, 2 and 3 – step from 50 to 75% of full-load

Figure 7-4: Active power of phase 1, 2 and 3 – step from 75 to 100% of full-load

Among the other measured variables, the only one that is worth to analyze is the H_2 flow. In fact, the reactive power is not relevant for the purpose of analyzing the electrolyser dynamic behavior, since the change of H_2 flow setpoint only affects the active power consumption. Also the DC power of the stack is not considered in this context because, on one hand, no dynamic is visible from the performed measurements due to the maximum electrolyser software sample time of 5s; on the other hand, the power on the DC side must simply show the same dynamic behavior of the power measured on the AC side minus losses.

By looking at the graph in figure 7-5, showing the H_2 output flow for the 0–25% experiment, it can be observed that the dynamic lasts about 14s. This is quite slow due to the fact that the start-up phase is still ongoing, thus the electrolyser unit is still building up pressure. In contrast, from the graph in figure 7-6 which illustrates the H_2 output flow for the 25–50% experiment, it is possible to see a very fast dynamic with less than 1s duration. This case is also representative of the 50–75% and 75–100% experiments, in which the H_2 output flow is shown to change within the interval of 1s as well.
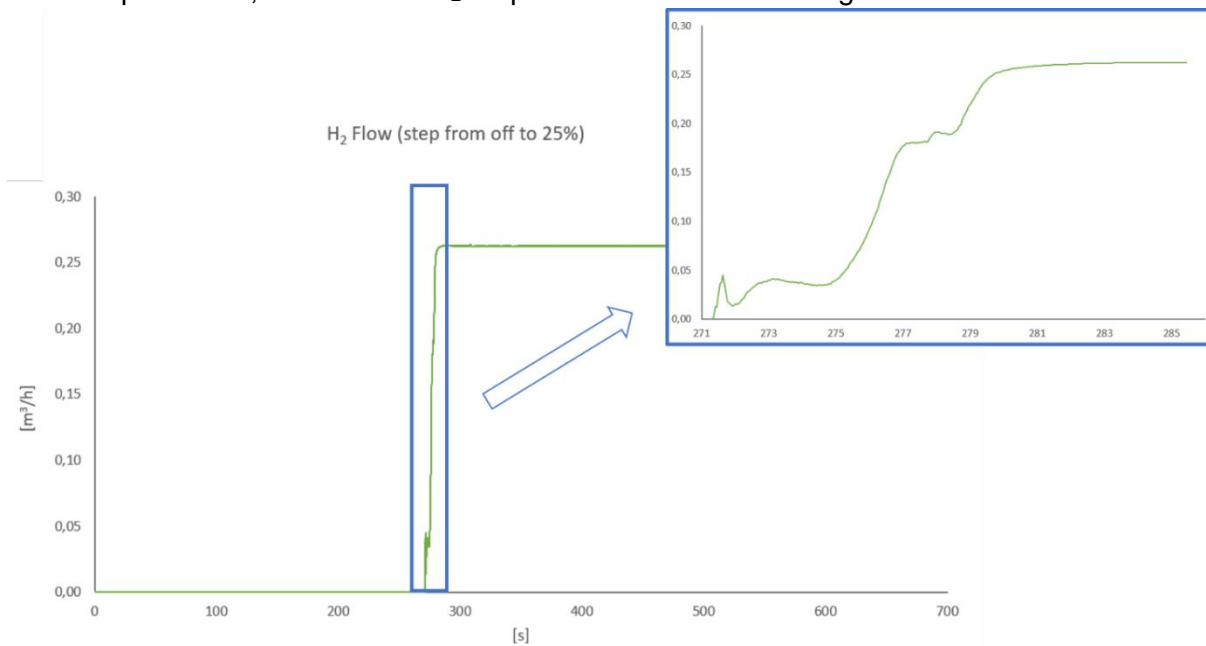

Figure 7-5: H_2 output flow – start-up and step to 25% of full-load (with zoom)
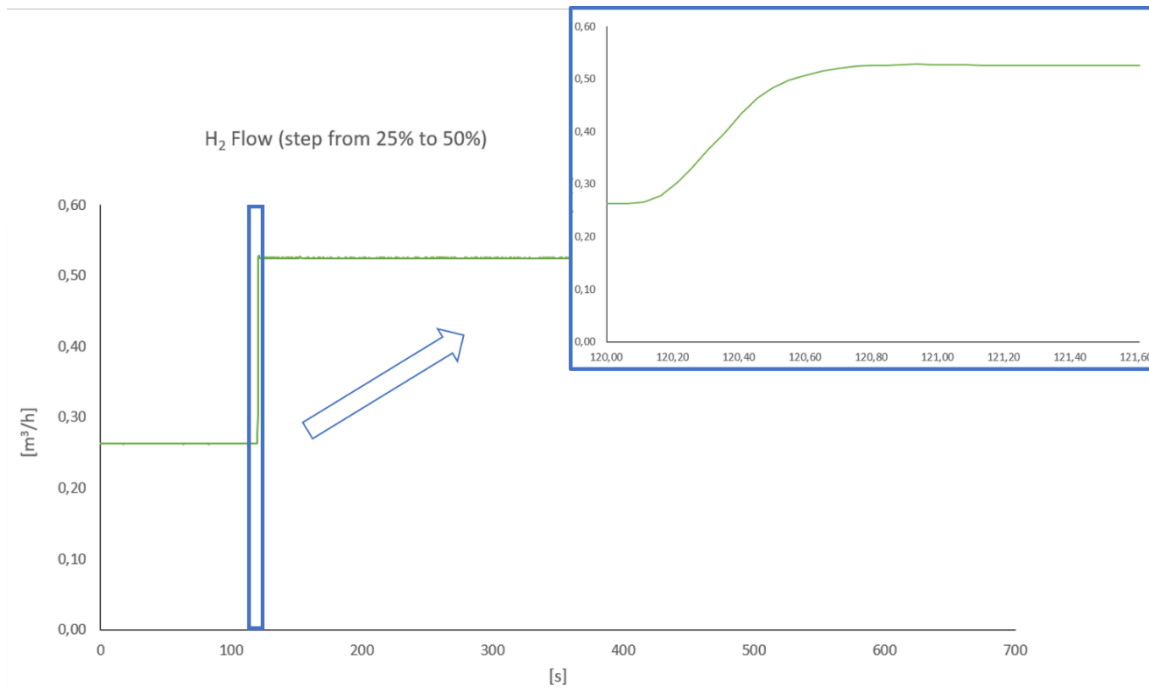
Figure 7-6: H_2 output flow – step from 25 to 50% of full-load (with zoom)

In conclusion, it is possible to state that the dynamic response of active power consumption is almost instantaneous. Therefore, the model constructed with the aim of mirroring the electrolyser electrical behavior through a static approach does not need to be modified, unless the start-up phase is needed to be introduced.

As a side comment, also the H_2 output flow shows a dynamic response very close to a step change when the electrolyser start-up has been completed. This means that, if the dynamic close to the start-up phase is not considered, the H_2 flow profile resulting from the switching between the waveforms included in the static version of the model is not too different from the real H_2 output flow.

7.1   Validation of the model

In order to demonstrate the validity of the model, the same four tests performed on the real electrolyser were carried out within the Simulink simulation and the final results were compared. Basically, the H_2 flow set points given to the flow controller through the mentioned software interface were saved in Matlab by means of the implemented code. This code also allows the conversion of the set points from the range of values needed for the flow controller Modbus communication to the range 0.25–1 (meaning from 25% to 100% of full-load). These waveforms were then passed from Matlab to Simulink and given as input control signals to the electrolyser model. The *Electrolyser* subsystem previously shown in figure 6-16 was modified as illustrated in figure 7-8. Here, the From Workspace block stores the *flow_setpoint* variable which case by case contains the described setpoint signal for each of the four step change experiments.
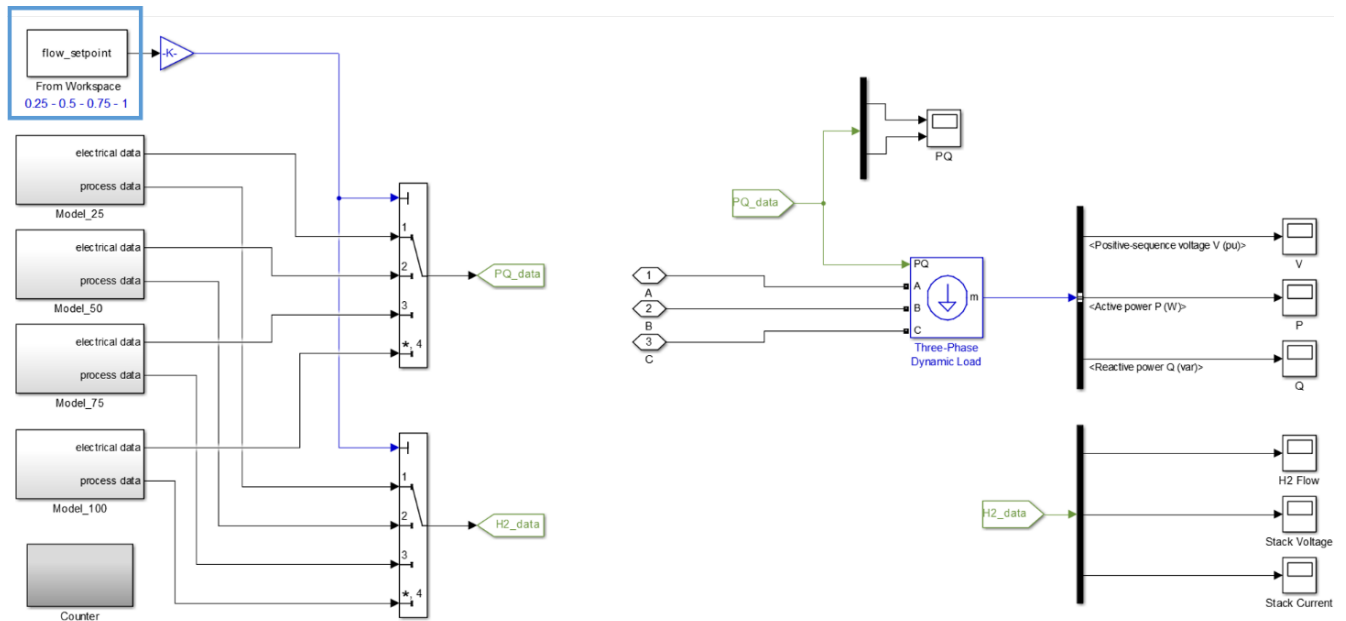
Figure 7-8: Electrolyser subsystem with flow_setpoint control signal

For all the analyzed cases, the patterns of both active and reactive power of all three phases resulting from the simulation are depicted in figures from 7-9 to 7-12. These are accompanied by the graphs of active power (already analyzed in the previous section) and reactive power which together show the electrical behavior of the real electrolyser. In this way, it is possible to carry out a final comparison.

In particular, in the comparative analysis of the results, it is necessary to focus on the power profiles of phase 1 as the only one used by the converter to rectify the stack voltage. In this way, it is visible that the waveforms representing the active power consumption of the simulated are only slightly shifted if compared to the real data. On this regard, it is worth to highlight that the real electrolyser behavior is not perfectly reproducible because shifts in the power consumption at a certain instant will anyway show up at different start-ups depending on the switching control initial instant. Another difference is constituted by the start-up phase. This can be observed from the graph of the 0–25% real case (marked in yellow), while in the simulated case it has not been electrolyser considered. In conclusion, since the real and simulated data are generally comparable, it can be stated that the model built with the purpose to simulate the AC electrical behavior of the electrolyser without considering the system start-up is valid.
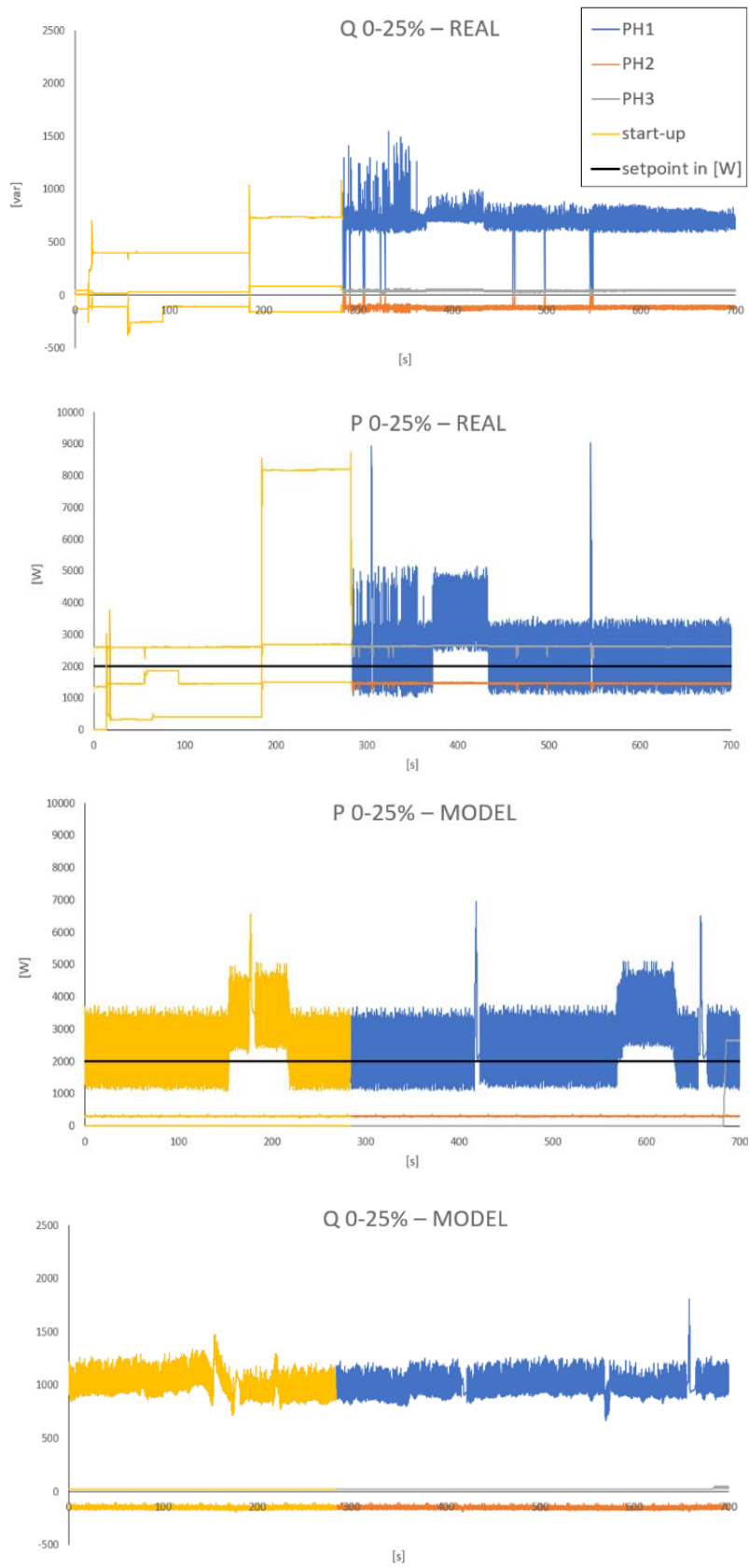
Figure 7-9: Comparison between real and simulated power profiles (case 0–25%)
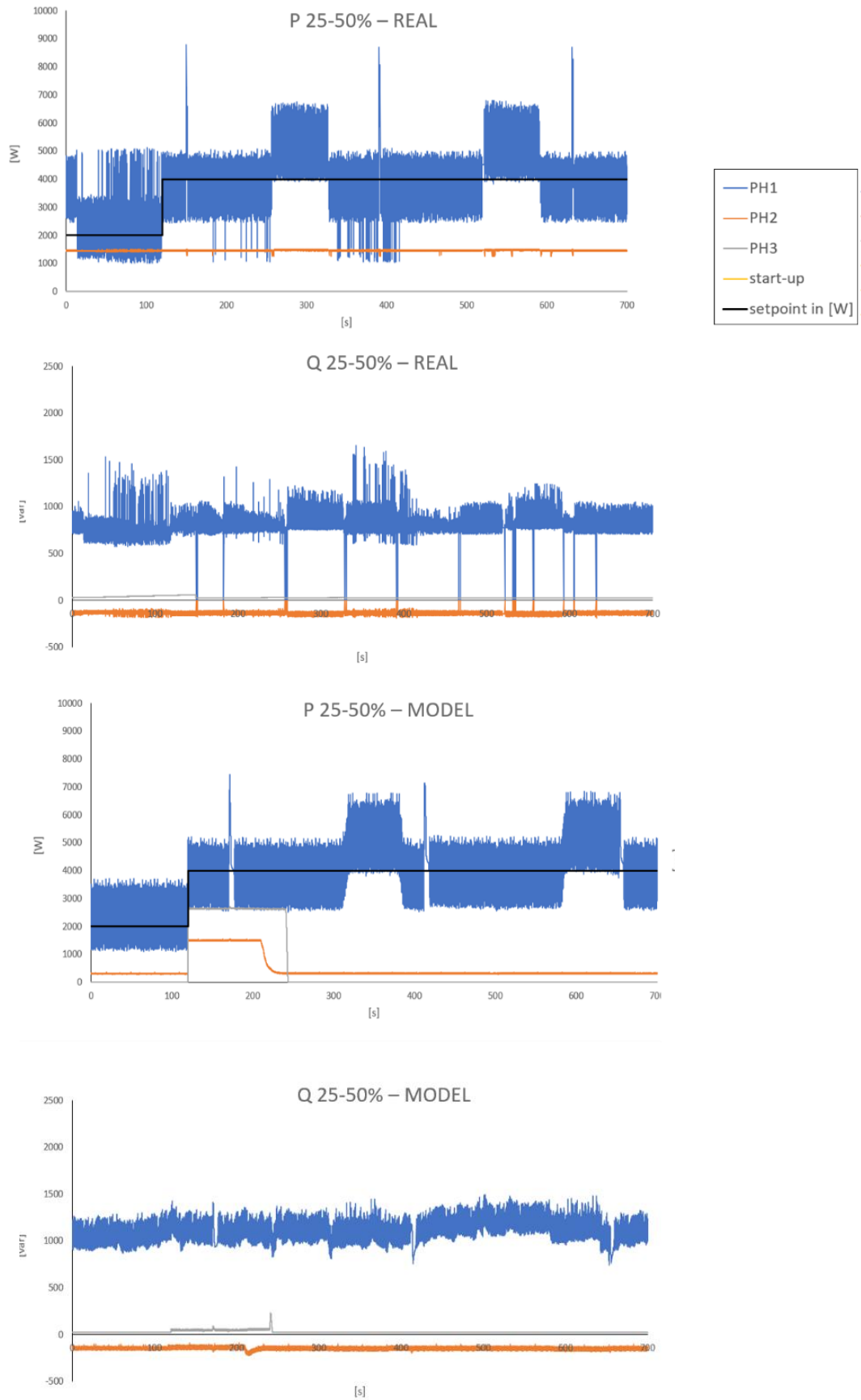
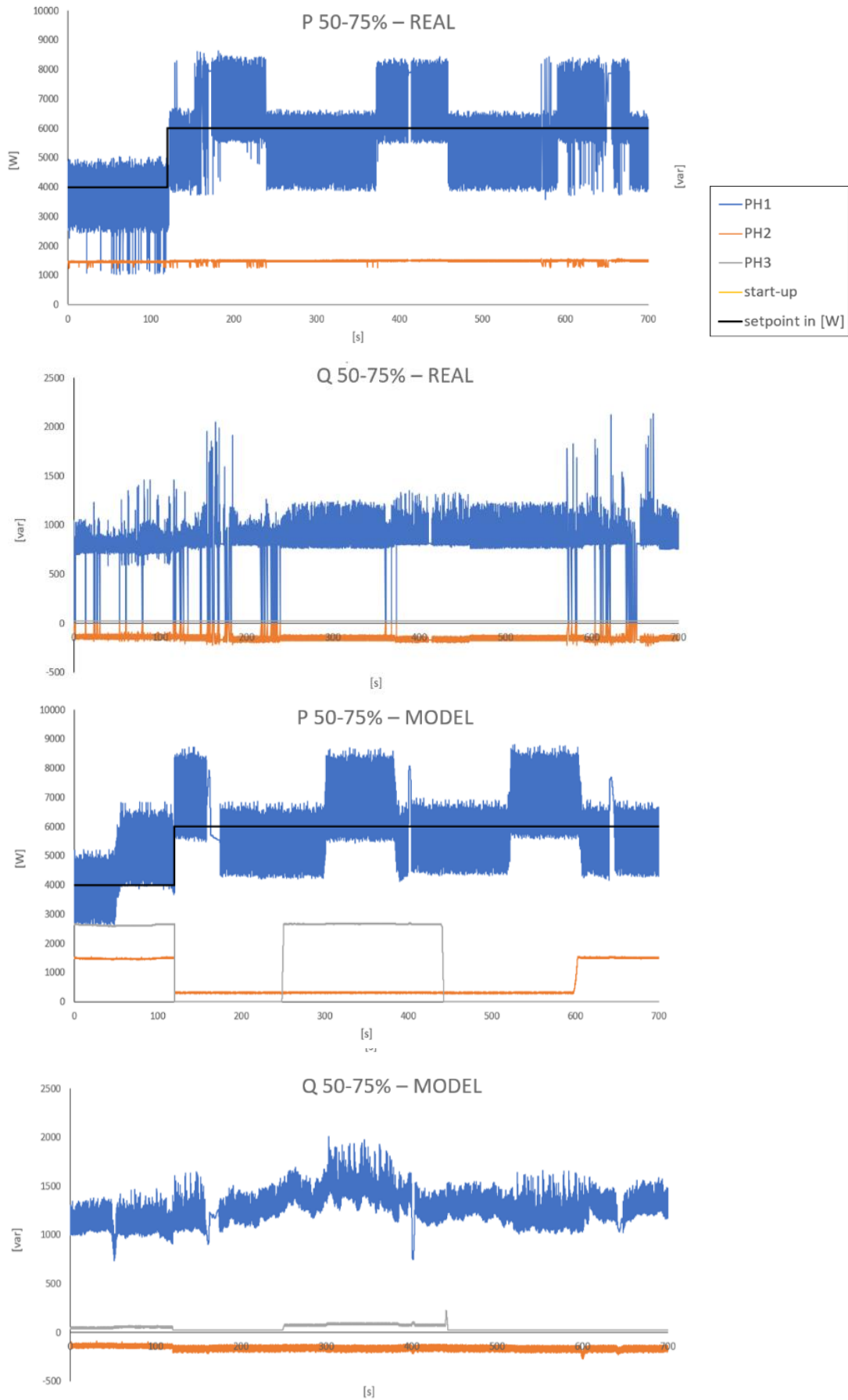**Figure 7-10:** Comparison between real and simulated power profiles (case 25–50%)

Figure 7-11: Comparison between real and simulated power profiles (case 50–75%)
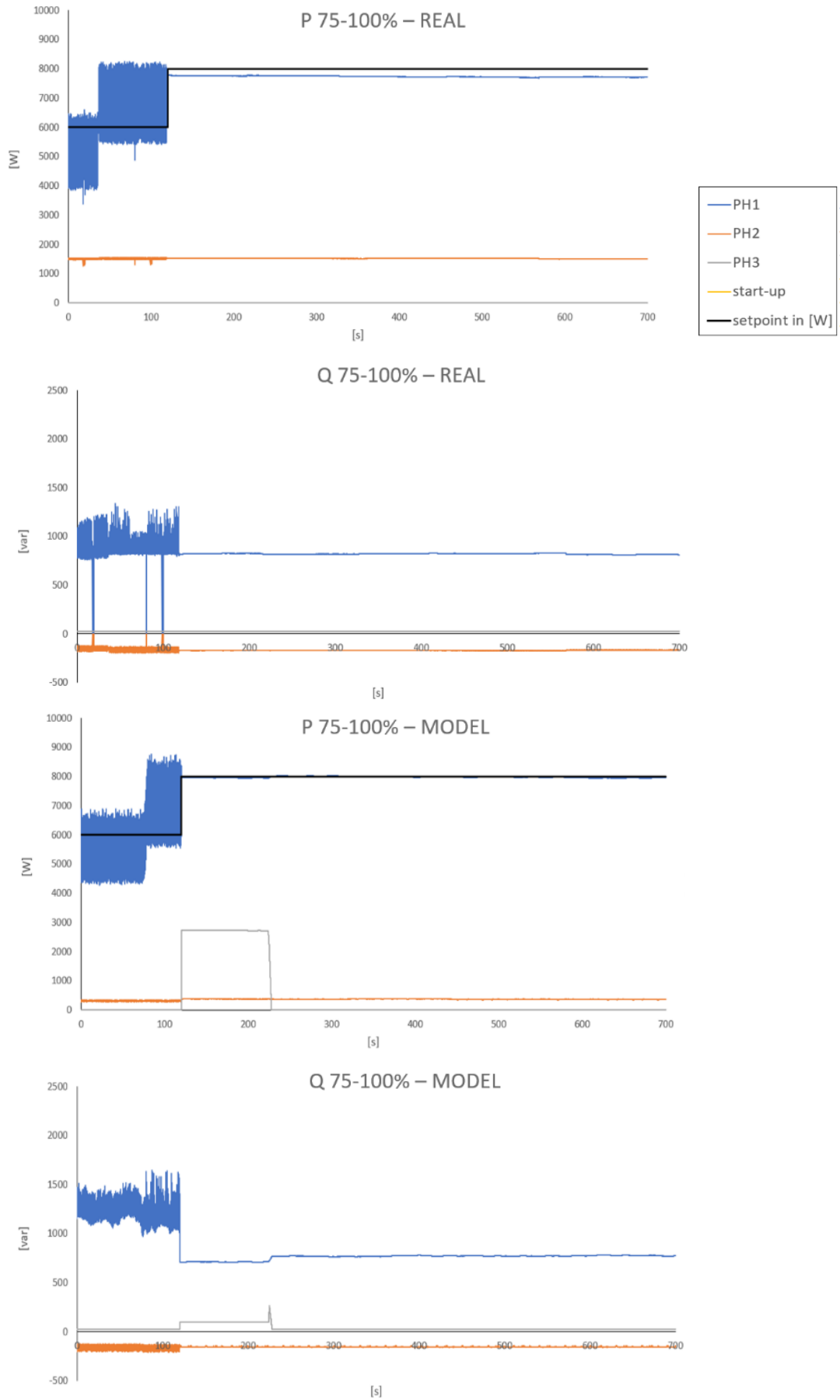
Figure 7-12: comparison between real and simulated power profiles (case 75–100%)

8   Results remote physical hardware in the loop

With the realized network configuration (chapter 4), the hardware installed on site is fully and safely controllable from the remote side. With this setup and the interoperability of the Triphase PM, it will be possible to connect the electrolyser as HIL into remote running simulations, finally realizing the so-called distributed real-time co-simulation. This chapter describes the test and results of remote physical hardware in the loop. With the implementation and use of the previously described connection:

- enables the remote access from PoliTo of the hardware and software resources located at Entrance micro grid setup , achieving the objective of the share of research infrastructures;
- offers the possibility to remotely monitor and control the set-up from within running simulations, which constitutes the first step towards a co-simulation involving RPHIL tests on the electrolyser.

The two experimental sets described in the following section were aimed at proving the feasibility of these two aspects.

8.1   Test: Inter-operability hard- software and VPN

The first experimental set was intended to demonstrate the functioning of the VPN communication for retrieving measurements from and sending control signals to the instruments, with a special attention payed to the data transmission delay. On these basis, two identical tests were performed by acting on the control and measurement equipment of the electrolyser, first locally from Groningen and then remotely from Turin. Specifically, the following operations were performed:

Control and measurement of the hydrogen flow rate (output) by means of the flow controller

The setpoint given to the flow controller in both cases was as follows: the electrolyser was started up with the flow controller set to 25% of maximum flow rate and this value was kept constant for 7 minutes to make sure that the electrolyser had been correctly started and the steady state had been reached; then 3 subsequent steps of 1 minute duration increased the setpoint of 25% at a time (1 minute at 50%, 1 minute at 75% and finally 1 minute at 100% of the maximum flow rate). The control was done by means of the Modbus controller setpoint software, while the data logging and saving were possible for both setpoint and real signals by using the implemented Matlab code.

Measurement of the active and reactive power (electrical input on the AC side) by means of the PPA power analyzer

The electrical inputs to the electrolyser were measured by means of the power analyzer, interfaced with its data logger software. The instrument was set by enabling High-Speed Mode and loading the same settings configuration already used during all the previous experiments at 20ms time step.

In this way, by using the software programs that come with the measuring devices, it was possible to set the sample time of both the instruments to the lowest value that they are capable to handle. The most relevant results obtained are shown in the following figures.
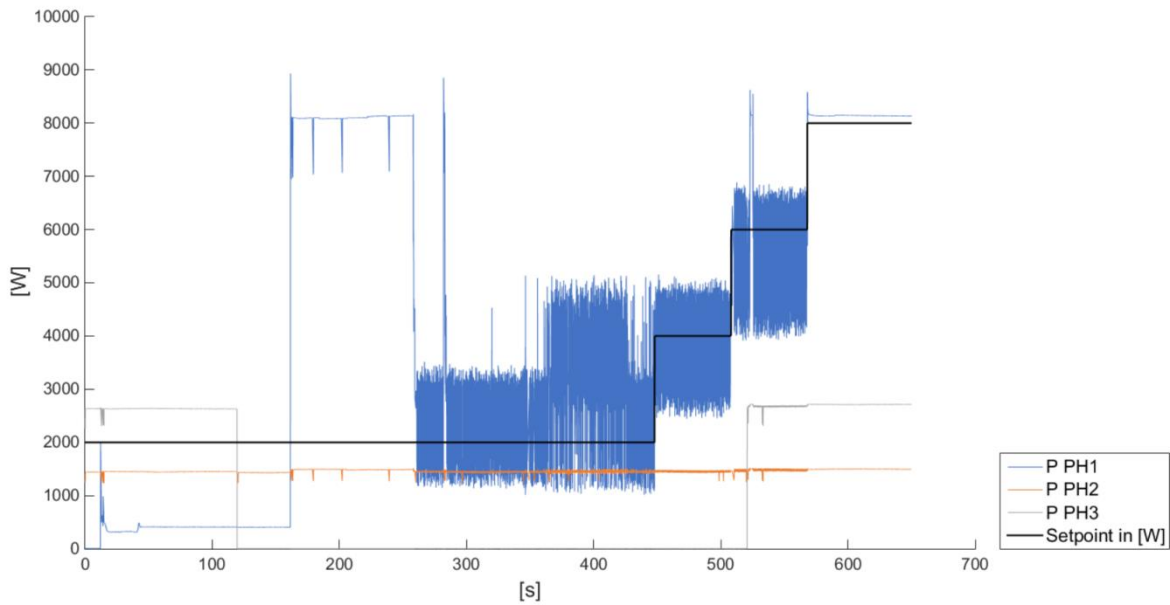
Figure 8-1: Active power withdrawn by the electrolyser - Local measurements
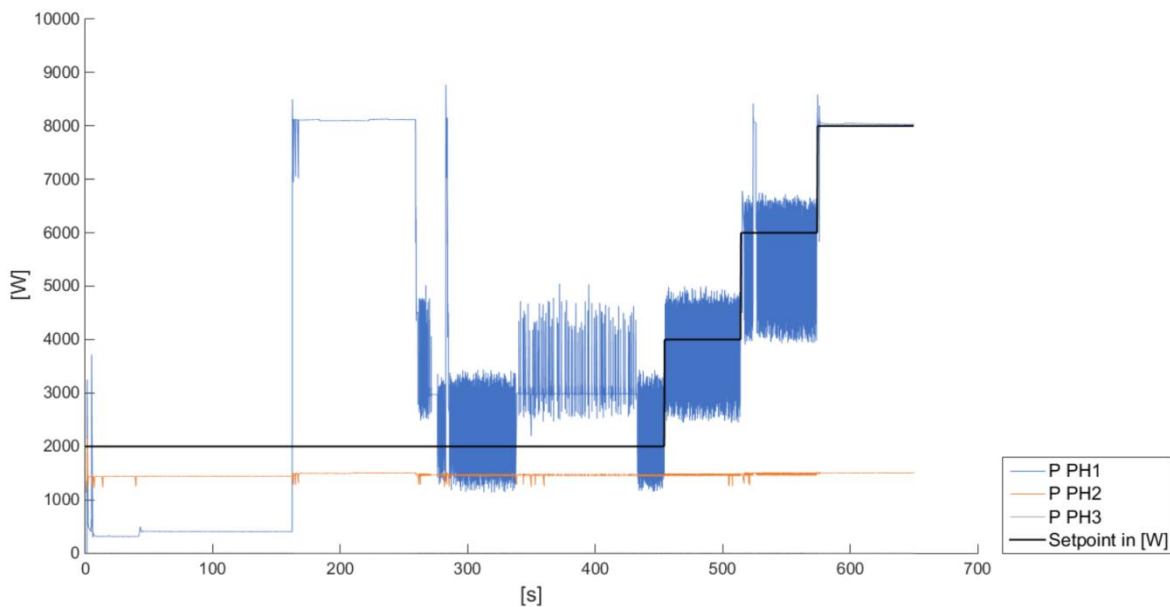

Figure 8-2: Active power withdrawn by the electrolyser - RHIL measurements

Figure 8.1 illustrates the active power for all three phases with measurements performed locally from Groningen, while Figure 8.2 depicts the same parameters with data logging carried out in remote from Turin. By looking at the graphs and focusing on phase 1 (which is the most important as the only phase used for rectifying the DC voltage) no big differences are visible between the local and remote measurements. In both cases the electrical behavior of the electrolyser passing through the same operating states is captured: the generating-vent mode with a low power consumption (around 400 W); the pressurize-storage state during which full power is applied to the stack (8 kW); the steady state at three partial load conditions (25, 50, 75%), in which the power profile variates around a mean value roughly equal to, respectively, 25, 50 or 75% of the maximum power consumption; at last, the steady state at full-load, in which the power is maintained constant and equal to the maximum value (8 kW). This is the well-known dynamic behavior of the electrolyser: the simple visual comparison of

the results has shown it can be captured from a remote location in the same way as on-site. In fact, the slight discrepancies emerging by comparing the two cases do not appear to be due to communication delays, but only to the fact that the electrolyser behavior is not perfectly reproducible at subsequent start-ups. (For instance, the generating-vent mode can last longer depending on the initial water quality, the waveforms representing the power consumption at a certain time can be shifted depending on the switching control initial instant and so on.)
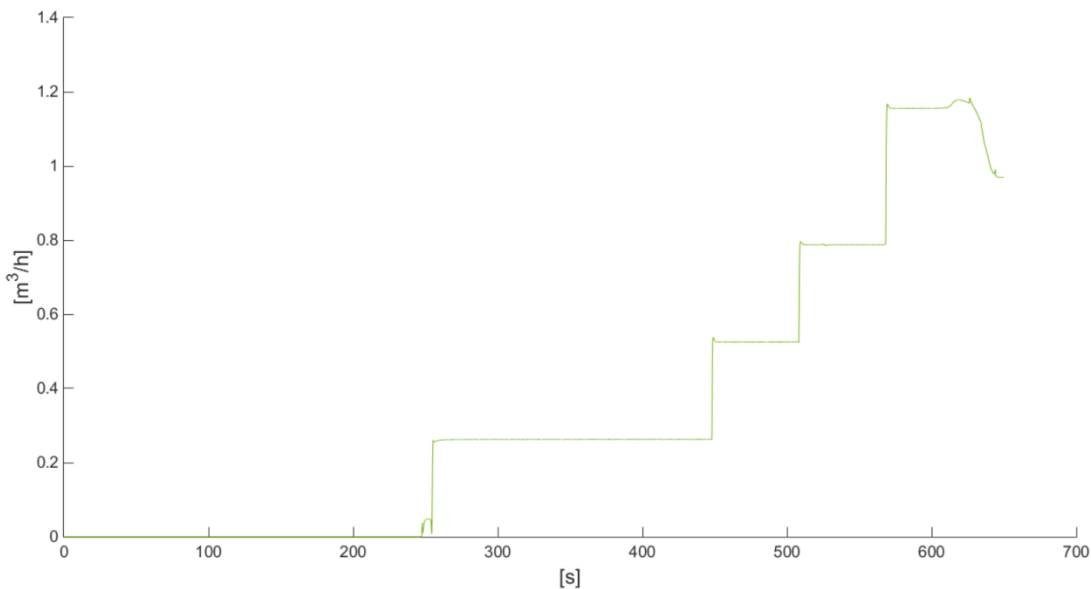

Figure 8-3: Production of H_2 - Local measurements
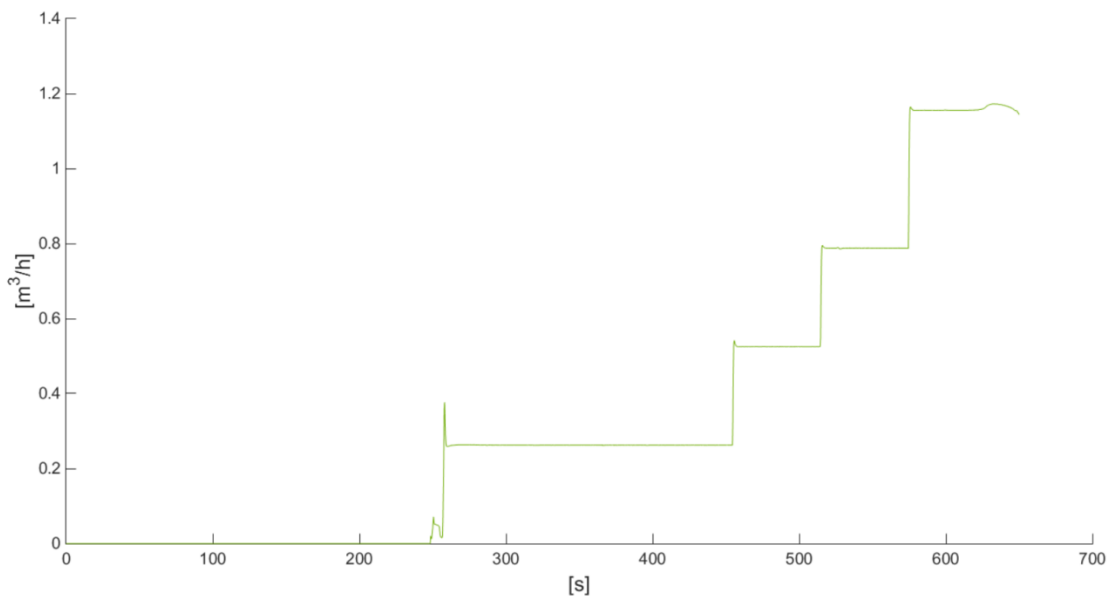

Figure 8-4: Production of H_2 - RHIL measurements

The hydrogen output flow measured both from Groningen and from Turin is presented in Figure 8.3 whereas the same parameter measured from Turin in shown in Figure 8.4 In both cases it can be seen the dynamic behavior of the flow passing through the steady state at the four load conditions (25, 50, 75, 100% of the maximum output flow – averaged to 1.05 m^3/h) with a dynamic between the steady states that lasts no more than 1s. Here again, it is possible to say that the two graphs are

very similar, the dynamic of the flow can be captured without any visible difference between the remote and the local measurements.

Since the delay due to the data transmission via VPN between the two laboratories could not be inferred from a comparison of the graphs, it was necessary to pay attention to the logging time of the instruments and, for a further analysis, to look deeply into the packets exchange by using WireShark [12] software for network protocol analysis. From such analysis, it emerged that:

Power analyzer: the minimum sampling time handled locally is 20 ms and it can be respected on average when the instrument is read in remote. This is due to the way in which the High-Speed measurement mode is implemented [12]: the power analyzer is able to sequentially send the data packets to the PC without any need for query. It follows that, since the speed of the forwarded data is higher than the latency of the communication link, the packets are queued and then received at irregular intervals.

Flow controller: the minimum transaction time for the control through Modbus interface equals 30ms from Groningen and rises to about 100ms from Turin. The minimum sampling times for the measurements through the implemented code in Matlab are 50 ms from Groningen and 140 ms from Turin[3]. This slight delay is due to the fact that the communication of the instrument is based on a normal Modbus TCP/IP protocol [10], so that the request from the remote PC must be received before the instrument could send back the reply.

In conclusion, the latency introduced by the VPN communication only slightly affects the remote measurements in terms of regularity of the time step for the power analyzer and minimum sampling time for the flow controller. Also the transaction time for the remote control of the flow controller setpoint is marginally influenced. Nevertheless, the delays introduced in the entire control chain are minimal and do not prevent the use of the multi-site set-up for research purposes.

8.2   Test: Mathematical model inter-operability

The second series of experiments was aimed at carrying out the control and measurement of electrolyser data from within a Matlab Simulink environment, both locally and remotely, in order to demonstrate the possibility of integrating the hydrogen production unit into co-simulations on the basis of RHIL concepts. A Simulink model was created for this purpose, which is composed of three different conceptual parts:

Flow controller Modbus writing: used to read the measured data of H_2 flow from the flow controller;

Flow controller Modbus reading: used to write the setpoint of H_2 flow from the flow controller;

Power analyzer TCP reading: used to read the three-phase active and reactive power from the power analyzer.

Each part contains Matlab functions implemented on purpose either for writing or reading the data of the respective instrument, taking into account the protocol requirements and also the necessary translation (may be ASCII, binary, decimal or hexadecimal). The three component parts of the Simulink model are shown in Figures from 8-5 to 8-7

---

[3] when the code is only used to log the measured data. Otherwise, if the code is used to log both setpoint and measured data the minimum sampling time equals 80ms from Groningen and 280ms from Turin.
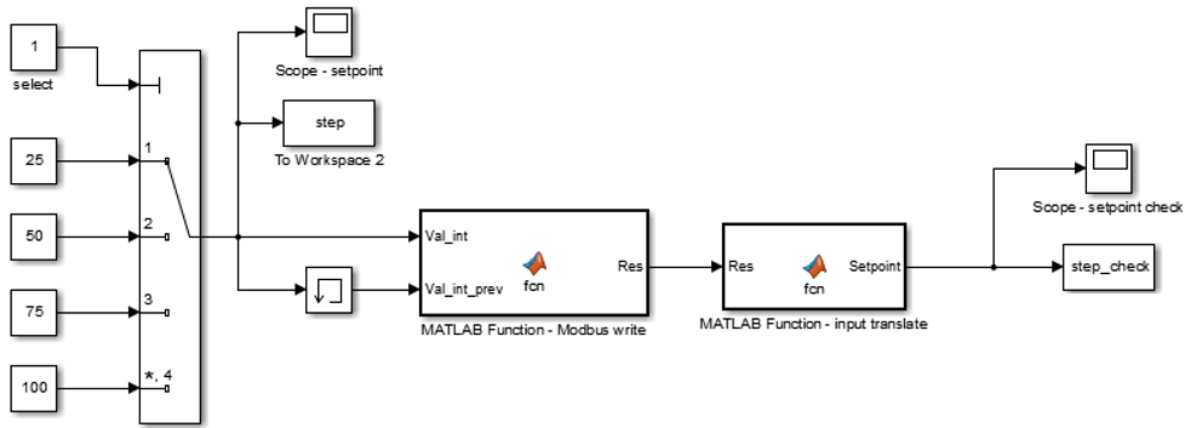
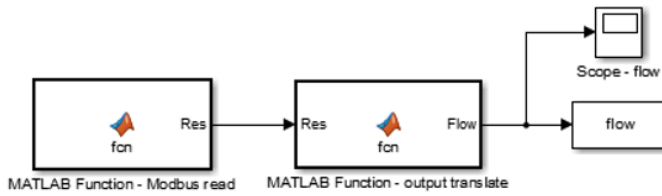**Figure 8-5:** Simulink model subsystem: flow controller Modbus writing

p

Figure 8-6: Simulink model subsystem: flow controller Modbus reading
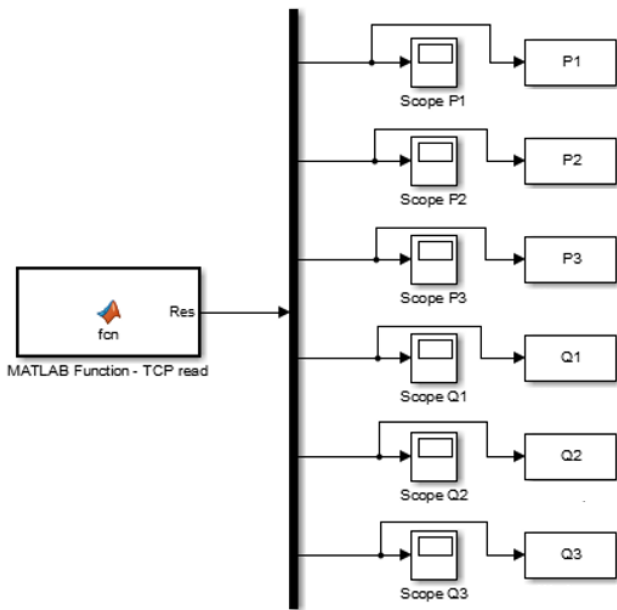

Figure 8-6: Simulink model subsystem: power analyzer TCP reading

With this model, two identical tests were performed by giving the flow controller the same setpoint already described in the previous section, first locally from Groningen and then remotely from Turin.
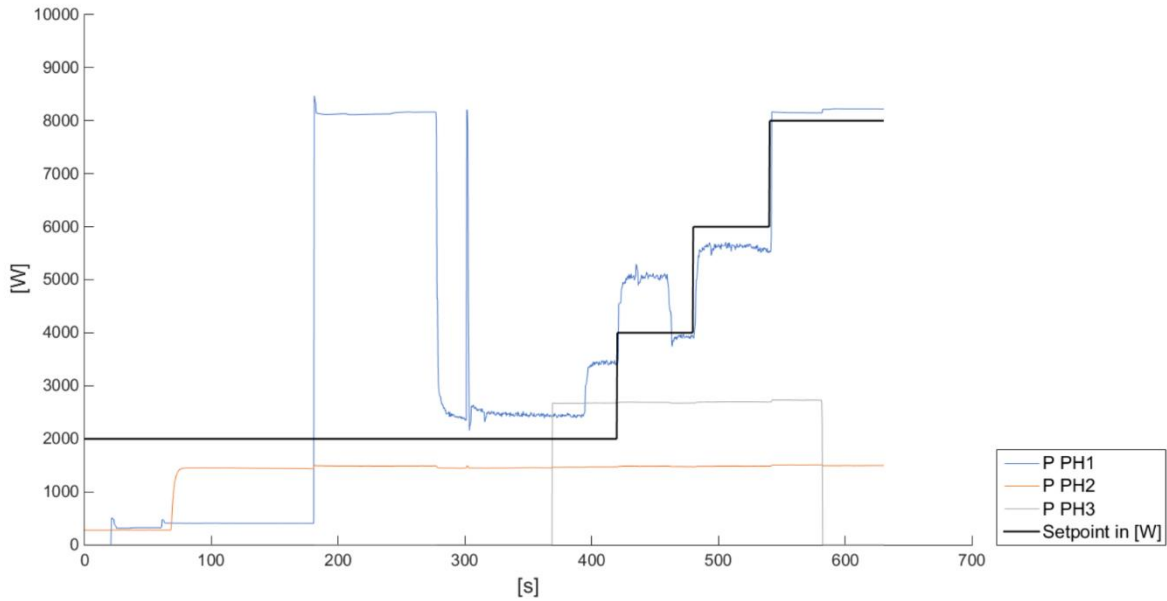
Figure 8-7: Active power withdrawn by the electrolyser - Local model measurements
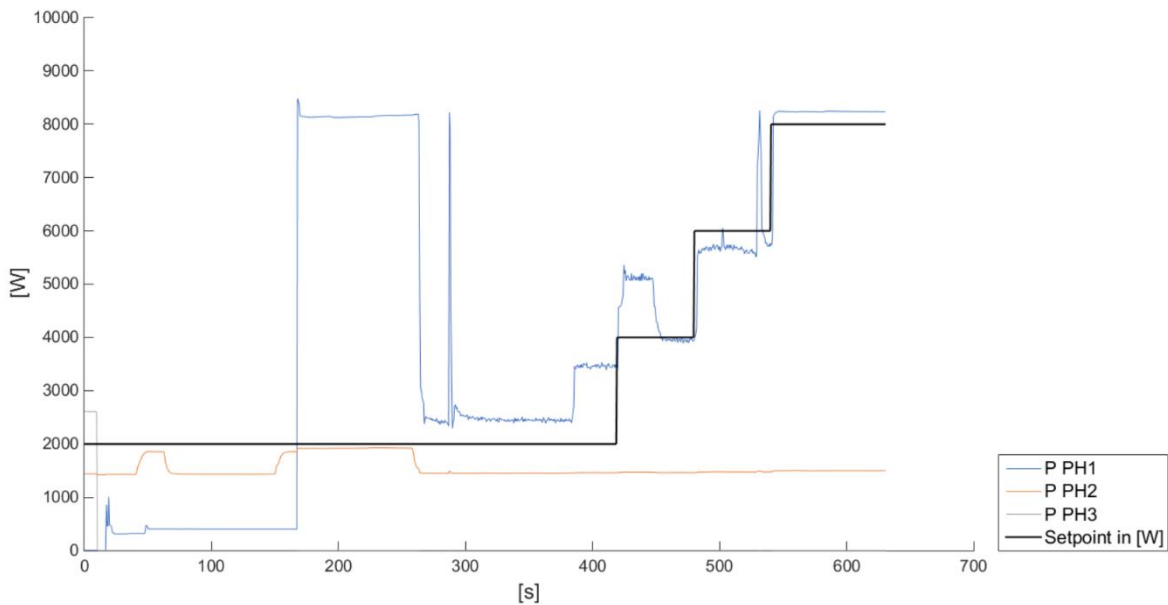

Figure 8-8: Active power withdrawn by the electrolyser - RHIL Simulink model measurements

The results obtained for the three-phase active power are shown in Figure 8.7 (model run from Groningen), and in Figure 8-8 (model run from Turin).

All the considerations on the electrolyser dynamic behavior presented in the above section are still valid here. From both graphs, by focusing of phase 1, it can be observed the electrolyser startup phase comprising generating-vent and pressurize-storage states; then the steady states steady state at 25, 50, 75 and 100% of full-load, with an almost step change in between them. The only main difference highlighted in these cases is that the ranges of power variation are consistently reduced if compared with the results of the previous experimental set. The measured values at each time step appears to be the only an average of the real data within the considered interval.

This is due to the fact that, within the Simulink environment, the instruments cannot be read at the minimum sample time available as in the first cases, but this has to be necessarily higher because of the further latency introduced by the simulation. In fact, it is worth to notice that the Simulink block Matlab Function works by interacting with Matlab while running the simulation. At each simulation time step the model is momentarily paused, the Simulink blocks interface with the respective Matlab file that runs the code to read/write data from and to the instruments. Finally, when the values are received, they are transferred from Matlab to Simulink and the simulation starts again moving to the subsequent time step.

This increased the minimum simulation time step to 400 ms when the model was run from Groningen. When the same model was run from Turin, the latency due to the communication Matlab-Simulink in addition to the delay due to the VPN communication further raised the minimum simulation time step to 600 ms.[4] In both cases, this is the minimum fixed-step time it was possible to set. In fact, since the simulation time step also identify the time period in which new values are requested and received from the instruments, a lower value would create too much data traffic which would slow down the communication and eventually lead to failure in the instruments and simulation crash.
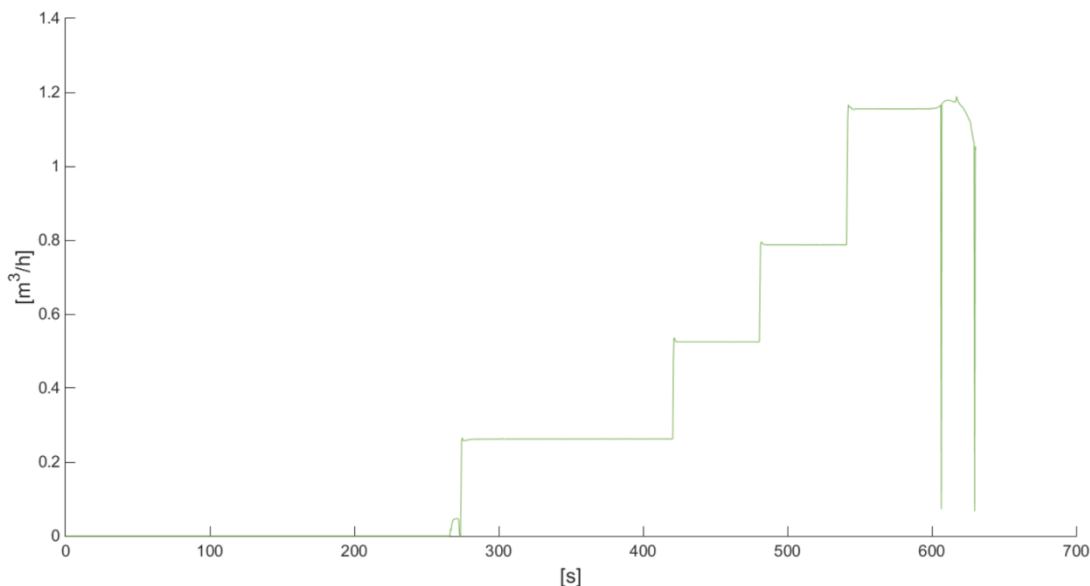

Figure 8-9: Simulink model subsystem: flow controller Modbus writing

---

[4] The simulation was performed as a normal non-real-time simulation, with the simulation time step set to 25 ms. The simulation duration was timed and the time step scaled up to real-time.
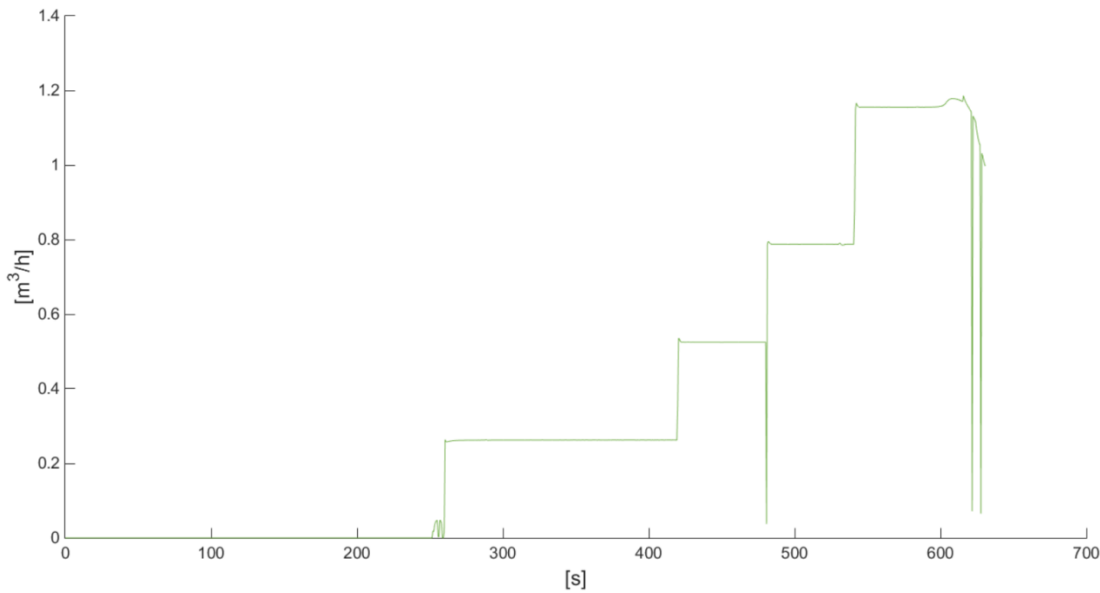
Figure 8-10: Production of H_2 – RHIL model measurements

At last, the measurements of hydrogen output flow are presented in Figure 8-9 (model run from Groningen) and in Figure 8-10 (model run from Turin). The two graphs are barely distinguishable from the respective graphs obtained during the previous test case. In fact, unlike the power read from the power analyzer, the H_2 flow obtained from the flow controller is generally not influenced by the huge increment in time step due to the simulation latency. This is because the flow is constant during the steady states and does not present the variation typically analyzed for the power. Only the accuracy in capturing the flow dynamic, lasting less than 1s, might be influenced by the higher time step.

In conclusion, it is possible to manage the measurement and control chain of the electrolyser within a simulation running locally and – what is more important, remotely, but this leads to limits in terms of minimum sample time for reading the instruments and minimum simulation time step. In particular, this influences the accuracy in reading the power from the power analyzer while the reading of the flow controller is marginally affected only with regard to the capture of the flow dynamics. Improvements in the method of integrating the measuring and control devices in Simulink may lead to a lower simulation time step (for example by developing appropriate Simulink S-function blocks for interacting with the instruments without need to interface with Matlab).

9 Conclusions

The Deliverable explained in detail all the technical aspects concerning the creation of the physical infrastructure for remotely acting on the electrolyser at the Entrance facility, both in terms of control and measurements. The activities involved installing and testing the different infrastructure parts, as well as their connection. In particular, the main systems developed so far count in:

- Local electrical grid, which can be managed either connected to the main grid or in island mode. This infrastructure allows the connection of different components, aiming to replicate the "prosumer" environment, considering both loads and generation

- Measurement infrastructure, mainly composed of the power analyser, able to properly measure with high sampling rate electrical variables (i.e., active and reactive power, current and so on), in such a way that the dynamic behaviour of the electrolyser could be captured and used later in simulations

- Communication infrastructure, for sending in quasi-real time the collected measurements, but also for sending the control signals for changing the operative conditions of the electrolyser

- Control system, up to now acting only on the flow controller. This control allows to modify the production of hydrogen, i.e., studying how the system react in case of change of the production. In the future, the control system will act also directly on the electrical inputs (AC side), for replicating the network conditions simulated in another platform (i.e., real time simulator). The modification of the electrical inputs will be reached through the supply of the entire system through a power amplifier, already installed in Hanze and for which a Simulink model is under design

The test field developed is, up to know, applied to a small scale plant, but it demonstrates the possibility to use this kind of infrastructure to collect information (in real time) also from larger plants, such as the ones installed in the demo site. This opens the possibility to use the data for research purposed, but also to act in remote on the infrastructure in case of particular test (for example the acceptance test).

The next steps will be focused on the control of the electrical variables trough the power amplifier, as well as the creation of proper tests using the entire infrastructure as Hardware-in-the-loop.

References

[1]   M. D. Omar Faruque et al., "Real-Time Simulation Technologies for Power Systems Design, Testing, and Analysis," in IEEE Power and Energy Technology Systems Journal, vol. 2, no. 2, pp. 63-73, June 2015. doi: 10.1109/JPETS.2015.2427370

[2]   X. Guillaud et al., "Applications of Real-Time Simulation Technologies in Power and Energy Systems," in IEEE Power and Energy Technology Systems Journal, vol. 2, no. 3, pp. 103-115, Sept. 2015. doi: 10.1109/JPETS.2015.2445296

[3]   JRC report, "A European Platform for Distributed Real Time Modelling & Simulation of Emerging Electricity Systems", 2016, http://publications.jrc.ec.europa.eu/repository/bitstream/JRC101772/reqno_jrc101772_rtms%20platform%20-%202016.pdf

[4]   STORE&GO, "D6.2: Status PtG grid integration experiments"

[5]   G. Chicco, V. Cocina, V. and A. Mazza, "Data pre-processing and representation for energy calculations in net metering conditions", 2014 ENERGYCON 2014 - IEEE International Energy Conference pp. 413-419

[6]   F. Spertino, F. Corona, P. Di Leo, "Limits of Advisability for Master–Slave Configuration of DC–AC Converters in Photovoltaic Systems", IEEE Journal of Photovoltaics, Vol.2(4), Oct. 2012, pp. 547–554

[7]   STORE&GO, "D6.4: Report on the model of the power system with PtG"

[8]   Matlab Simulink developed by MathWorks, is a graphical programming environment for modeling, simulating and analyzing multidomain dynamical systems. Its primary interface is a graphical block diagramming tool and a customizable set of block libraries. It offers tight integration with the rest of the MATLAB environment and can either drive MATLAB or be scripted from it. Simulink is widely used in automatic control and digital signal processing for multidomain simulation and Model-Based Design Matlab, Simulink are registered trademarks . https://nl.mathworks.com/products/simulink.html

[9]   Triphase HPC Explained white paper, Shaping dynamic response using virtual circuit control ,Triphase N.V., 2014

[10]   A.S. Tannenbaum , Computer networks, 2003. ISBN 90-430-0698-X

[11]   PPA - Newtons4th Ltd (abbreviated to N4L) was established in 1997 to design, manufacture and support innovative electronic equipment to a world-wide market...

[12]   Newtons4th LTd, PPA5xx-15xx-communications manual, April 4 2017

[13]   https://www.wireshark.org/

[14]   Website STORE&GO: https://storeandgo.info/

[15]   OPAL is a trademark of OPAL technologies. https://www.opal-rt.com/

[16]   Triphase is a registered trademark of National Instruments. https://triphase.com/